EUROPEAN LABORATORY FOR PARTICLE PHYSICS

CERN-PPE/97-036
2 April 1997

A Study of B Meson Oscillations Using Hadronic Z^0 Decays Containing Leptons

The OPAL Collaboration

Abstract

An event sample enriched in semileptonic decays of b hadrons is selected using an inclusive lepton selection from approximately 3.0 million hadronic Z^0 decays collected with the OPAL detector. This sample is used to investigate B meson oscillations by reconstructing a proper decay time for the parent of each lepton, using a jet charge method to estimate the production flavour of this parent, and using the lepton charge to tag the decay flavour. We measure the mass difference between the two B_d^0 mass eigenstates

$$\Delta m_d = 0.444 \pm 0.029 \,^{+0.020}_{-0.017}\ \mathrm{ps}^{-1}\ .$$

For the B_s^0 system, we find $\Delta m_s > 3.1\ \mathrm{ps}^{-1}$ at the 95% confidence level. This limit varies only a little if alternative limit setting approaches are adopted. Regions at higher Δm_s values are also excluded with some methods for setting the limit.

By studying the charge symmetry of the B_d^0 mixing structure, we are able to constrain possible CP and CPT violating effects. We measure the CP violation parameter

$$\mathrm{Re}\,\epsilon_B = -0.006 \pm 0.010 \pm 0.006$$

and the indirect CPT violating parameter

$$\mathrm{Im}\,\delta_B = -0.020 \pm 0.016 \pm 0.006\ .$$

If we invoke CPT symmetry, then we obtain

$$\mathrm{Re}\,\epsilon_B = 0.002 \pm 0.007 \pm 0.003\ .$$

(Submitted to Zeitschrift für Physik C)

The OPAL Collaboration

K. Ackerstaff[8], G. Alexander[23], J. Allison[16], N. Altekamp[5], K.J. Anderson[9], S. Anderson[12], S. Arcelli[2], S. Asai[24], D. Axen[29], G. Azuelos[18,a], A.H. Ball[17], E. Barberio[8], R.J. Barlow[16], R. Bartoldus[3], J.R. Batley[5], S. Baumann[3], J. Bechtluft[14], C. Beeston[16], T. Behnke[8], A.N. Bell[1], K.W. Bell[20], G. Bella[23], S. Bentvelsen[8], P. Berlich[10], S. Bethke[14], O. Biebel[14], A. Biguzzi[5], S.D. Bird[16], V. Blobel[27], I.J. Bloodworth[1], J.E. Bloomer[1], M. Bobinski[10], P. Bock[11], D. Bonacorsi[2], M. Boutemeur[34], B.T. Bouwens[12], S. Braibant[12], L. Brigliadori[2], R.M. Brown[20], H.J. Burckhart[8], C. Burgard[8], R. Bürgin[10], P. Capiluppi[2], R.K. Carnegie[6], A.A. Carter[13], J.R. Carter[5], C.Y. Chang[17], D.G. Charlton[1,b], D. Chrisman[4], P.E.L. Clarke[15], I. Cohen[23], J.E. Conboy[15], O.C. Cooke[16], M. Cuffiani[2], S. Dado[22], C. Dallapiccola[17], G.M. Dallavalle[2], S. De Jong[12], L.A. del Pozo[4], K. Desch[3], M.S. Dixit[7], E. do Couto e Silva[12], M. Doucet[18], E. Duchovni[26], G. Duckeck[34], I.P. Duerdoth[16], D. Eatough[16], J.E.G. Edwards[16], P.G. Estabrooks[6], H.G. Evans[9], M. Evans[13], F. Fabbri[2], M. Fanti[2], A.A. Faust[30], F. Fiedler[27], M. Fierro[2], H.M. Fischer[3], I. Fleck[8], R. Folman[26], D.G. Fong[17], M. Foucher[17], A. Fürtjes[8], D.I. Futyan[16], P. Gagnon[7], J.W. Gary[4], J. Gascon[18], S.M. Gascon-Shotkin[17], N.I. Geddes[20], C. Geich-Gimbel[3], T. Geralis[20], G. Giacomelli[2], P. Giacomelli[4], R. Giacomelli[2], V. Gibson[5], W.R. Gibson[13], D.M. Gingrich[30,a], D. Glenzinski[9], J. Goldberg[22], M.J. Goodrick[5], W. Gorn[4], C. Grandi[2], E. Gross[26], J. Grunhaus[23], M. Gruwé[8], C. Hajdu[32], G.G. Hanson[12], M. Hansroul[8], M. Hapke[13], C.K. Hargrove[7], P.A. Hart[9], C. Hartmann[3], M. Hauschild[8], C.M. Hawkes[5], R. Hawkings[27], R.J. Hemingway[6], M. Herndon[17], G. Herten[10], R.D. Heuer[8], M.D. Hildreth[8], J.C. Hill[5], S.J. Hillier[1], T. Hilse[10], P.R. Hobson[25], R.J. Homer[1], A.K. Honma[28,a], D. Horváth[32,c], R. Howard[29], D.E. Hutchcroft[5], P. Igo-Kemenes[11], D.C. Imrie[25], M.R. Ingram[16], K. Ishii[24], A. Jawahery[17], P.W. Jeffreys[20], H. Jeremie[18], M. Jimack[1], A. Joly[18], C.R. Jones[5], G. Jones[16], M. Jones[6], U. Jost[11], P. Jovanovic[1], T.R. Junk[8], D. Karlen[6], V. Kartvelishvili[16], K. Kawagoe[24], T. Kawamoto[24], R.K. Keeler[28], R.G. Kellogg[17], B.W. Kennedy[20], J. Kirk[29], A. Klier[26], S. Kluth[8], T. Kobayashi[24], M. Kobel[10], D.S. Koetke[6], T.P. Kokott[3], M. Kolrep[10], S. Komamiya[24], T. Kress[11], P. Krieger[6], J. von Krogh[11], P. Kyberd[13], G.D. Lafferty[16], R. Lahmann[17], W.P. Lai[19], D. Lanske[14], J. Lauber[15], S.R. Lautenschlager[31], J.G. Layter[4], D. Lazic[22], A.M. Lee[31], E. Lefebvre[18], D. Lellouch[26], J. Letts[12], L. Levinson[26], S.L. Lloyd[13], F.K. Loebinger[16], G.D. Long[28], M.J. Losty[7], J. Ludwig[10], A. Macchiolo[2], A. Macpherson[30], M. Mannelli[8], S. Marcellini[2], C. Markus[3], A.J. Martin[13], J.P. Martin[18], G. Martinez[17], T. Mashimo[24], P. Mättig[3], W.J. McDonald[30], J. McKenna[29], E.A. Mckigney[15], T.J. McMahon[1], R.A. McPherson[8], F. Meijers[8], S. Menke[3], F.S. Merritt[9], H. Mes[7], J. Meyer[27], A. Michelini[2], G. Mikenberg[26], D.J. Miller[15], A. Mincer[22,e], R. Mir[26], W. Mohr[10], A. Montanari[2], T. Mori[24], M. Morii[24], U. Müller[3], K. Nagai[26], I. Nakamura[24], H.A. Neal[8], B. Nellen[3], R. Nisius[8], S.W. O'Neale[1], F.G. Oakham[7], F. Odorici[2], H.O. Ogren[12], N.J. Oldershaw[16], M.J. Oreglia[9], S. Orito[24], J. Pálinkás[33,d], G. Pásztor[32], J.R. Pater[16], G.N. Patrick[20], J. Patt[10], M.J. Pearce[1], S. Petzold[27], P. Pfeifenschneider[14], J.E. Pilcher[9], J. Pinfold[30], D.E. Plane[8], P. Poffenberger[28], B. Poli[2], A. Posthaus[3], H. Przysiezniak[30], D.L. Rees[1], D. Rigby[1], S. Robertson[28], S.A. Robins[22], N. Rodning[30], J.M. Roney[28], A. Rooke[15], E. Ros[8], A.M. Rossi[2], M. Rosvick[28], P. Routenburg[30], Y. Rozen[22], K. Runge[10], O. Runolfsson[8], U. Ruppel[14], D.R. Rust[12], R. Rylko[25], K. Sachs[10], T. Saeki[24], E.K.G. Sarkisyan[23], C. Sbarra[29], A.D. Schaile[34], O. Schaile[34], F. Scharf[3], P. Scharff-Hansen[8], P. Schenk[34], J. Schieck[11], P. Schleper[11], B. Schmitt[8], S. Schmitt[11], A. Schöning[8], M. Schröder[8], H.C. Schultz-Coulon[10], M. Schulz[8], M. Schumacher[3], C. Schwick[8], W.G. Scott[20], T.G. Shears[16], B.C. Shen[4], C.H. Shepherd-Themistocleous[8], P. Sherwood[15], G.P. Siroli[2], A. Sittler[27], A. Skillman[15], A. Skuja[17], A.M. Smith[8], G.A. Snow[17], R. Sobie[28],

S. Söldner-Rembold[10], R.W. Springer[30], M. Sproston[20], K. Stephens[16], J. Steuerer[27], B. Stockhausen[3], K. Stoll[10], D. Strom[19], P. Szymanski[20], R. Tafirout[18], S.D. Talbot[1], S. Tanaka[24], P. Taras[18], S. Tarem[22], R. Teuscher[8], M. Thiergen[10], M.A. Thomson[8], E. von Törne[3], S. Towers[6], I. Trigger[18], E. Tsur[23], A.S. Turcot[9], M.F. Turner-Watson[8], P. Utzat[11], R. Van Kooten[12], M. Verzocchi[10], P. Vikas[18], E.H. Vokurka[16], H. Voss[3], F. Wäckerle[10], A. Wagner[27], C.P. Ward[5], D.R. Ward[5], P.M. Watkins[1], A.T. Watson[1], N.K. Watson[1], P.S. Wells[8], N. Wermes[3], J.S. White[28], B. Wilkens[10], G.W. Wilson[27], J.A. Wilson[1], G. Wolf[26], T.R. Wyatt[16], S. Yamashita[24], G. Yekutieli[26], V. Zacek[18], D. Zer-Zion[8]

[1]School of Physics and Space Research, University of Birmingham, Birmingham B15 2TT, UK
[2]Dipartimento di Fisica dell' Università di Bologna and INFN, I-40126 Bologna, Italy
[3]Physikalisches Institut, Universität Bonn, D-53115 Bonn, Germany
[4]Department of Physics, University of California, Riverside CA 92521, USA
[5]Cavendish Laboratory, Cambridge CB3 0HE, UK
[6] Ottawa-Carleton Institute for Physics, Department of Physics, Carleton University, Ottawa, Ontario K1S 5B6, Canada
[7]Centre for Research in Particle Physics, Carleton University, Ottawa, Ontario K1S 5B6, Canada
[8]CERN, European Organisation for Particle Physics, CH-1211 Geneva 23, Switzerland
[9]Enrico Fermi Institute and Department of Physics, University of Chicago, Chicago IL 60637, USA
[10]Fakultät für Physik, Albert Ludwigs Universität, D-79104 Freiburg, Germany
[11]Physikalisches Institut, Universität Heidelberg, D-69120 Heidelberg, Germany
[12]Indiana University, Department of Physics, Swain Hall West 117, Bloomington IN 47405, USA
[13]Queen Mary and Westfield College, University of London, London E1 4NS, UK
[14]Technische Hochschule Aachen, III Physikalisches Institut, Sommerfeldstrasse 26-28, D-52056 Aachen, Germany
[15]University College London, London WC1E 6BT, UK
[16]Department of Physics, Schuster Laboratory, The University, Manchester M13 9PL, UK
[17]Department of Physics, University of Maryland, College Park, MD 20742, USA
[18]Laboratoire de Physique Nucléaire, Université de Montréal, Montréal, Quebec H3C 3J7, Canada
[19]University of Oregon, Department of Physics, Eugene OR 97403, USA
[20]Rutherford Appleton Laboratory, Chilton, Didcot, Oxfordshire OX11 0QX, UK
[22]Department of Physics, Technion-Israel Institute of Technology, Haifa 32000, Israel
[23]Department of Physics and Astronomy, Tel Aviv University, Tel Aviv 69978, Israel
[24]International Centre for Elementary Particle Physics and Department of Physics, University of Tokyo, Tokyo 113, and Kobe University, Kobe 657, Japan
[25]Brunel University, Uxbridge, Middlesex UB8 3PH, UK
[26]Particle Physics Department, Weizmann Institute of Science, Rehovot 76100, Israel
[27]Universität Hamburg/DESY, II Institut für Experimental Physik, Notkestrasse 85, D-22607 Hamburg, Germany
[28]University of Victoria, Department of Physics, P O Box 3055, Victoria BC V8W 3P6, Canada
[29]University of British Columbia, Department of Physics, Vancouver BC V6T 1Z1, Canada
[30]University of Alberta, Department of Physics, Edmonton AB T6G 2J1, Canada

[31]Duke University, Dept of Physics, Durham, NC 27708-0305, USA
[32]Research Institute for Particle and Nuclear Physics, H-1525 Budapest, P O Box 49, Hungary
[33]Institute of Nuclear Research, H-4001 Debrecen, P O Box 51, Hungary
[34]Ludwigs-Maximilians-Universität München, Sektion Physik, Am Coulombwall 1, D-85748 Garching, Germany

[a] and at TRIUMF, Vancouver, Canada V6T 2A3
[b] and Royal Society University Research Fellow
[c] and Institute of Nuclear Research, Debrecen, Hungary
[d] and Department of Experimental Physics, Lajos Kossuth University, Debrecen, Hungary
[e] and Depart of Physics, New York University, NY 1003, USA

1 Introduction

The phenomenon of $\mathrm{B}-\bar{\mathrm{B}}$ mixing is now well established. Particle-antiparticle oscillations arise when the weak eigenstates, $|\mathrm{B}^0\rangle$[1] and $|\bar{\mathrm{B}}^0\rangle$, differ from the mass eigenstates, $|\mathrm{B}_1\rangle$ and $|\mathrm{B}_2\rangle$, which can be described as follows:

$$\begin{aligned} |\mathrm{B}_1\rangle &= \frac{(1+\epsilon+\delta)|\mathrm{B}^0\rangle + (1-\epsilon-\delta)|\bar{\mathrm{B}}^0\rangle}{\sqrt{2(1+|\epsilon+\delta|^2)}} \\ |\mathrm{B}_2\rangle &= \frac{(1+\epsilon-\delta)|\mathrm{B}^0\rangle - (1-\epsilon+\delta)|\bar{\mathrm{B}}^0\rangle}{\sqrt{2(1+|\epsilon-\delta|^2)}}\,, \end{aligned} \tag{1}$$

where ϵ and δ are complex, and parametrise indirect CP and CPT violation [1]. Note that ϵ allows for CP and T violation while respecting CPT symmetry, and δ allows for CP and CPT violation, but respects T symmetry. This formalism applies to both the B^0_d and B^0_s systems, with separate values for ϵ and δ in each system. The mass difference, Δm_q, between the two mass eigenstates for the B^0_q-$\bar{\mathrm{B}}^0_\mathrm{q}$ system determines the frequency of oscillation, where B^0_q stands for either B^0_d or B^0_s. In the Standard Model, transitions between B^0_q and $\bar{\mathrm{B}}^0_\mathrm{q}$ mesons arise dominantly via box diagrams involving virtual top quarks. Predictions for the mass differences can be made, and depend on the top mass and the CKM elements V_tq. For the B^0_d system,

$$\Delta m_\mathrm{d} \propto f^2_{\mathrm{B}^0_\mathrm{d}} B_{\mathrm{B}^0_\mathrm{d}} m_\mathrm{t}^2 F(m_\mathrm{t}^2) |V_\mathrm{td} V_\mathrm{tb}^*|^2 \tag{2}$$

where the first two factors are the meson decay constant and QCD bag model vacuum insertion parameter, respectively. These factors are obtained from lattice QCD calculations and QCD sum rules, but there is an uncertainty of the order of 50% on this product [2]. The next two factors are the top quark mass, m_t, and a known quadratic function of m_t. The last factor is a product of CKM matrix elements. At this point, an accurate measurement of Δm_d alone would not lead to an accurate result for V_td because of the uncertainty in the decay and bag constants. However, if both Δm_d and Δm_s could be measured then information on the CKM matrix could be extracted via the ratio

$$\frac{\Delta m_\mathrm{s}}{\Delta m_\mathrm{d}} = \frac{m_{\mathrm{B}^0_\mathrm{s}}}{m_{\mathrm{B}^0_\mathrm{d}}} \cdot \frac{|V_\mathrm{ts}|^2}{|V_\mathrm{td}|^2} \cdot \frac{f^2_{\mathrm{B}^0_\mathrm{s}} B_{\mathrm{B}^0_\mathrm{s}}}{f^2_{\mathrm{B}^0_\mathrm{d}} B_{\mathrm{B}^0_\mathrm{d}}}\,, \tag{3}$$

where $m_{\mathrm{B}^0_\mathrm{s}}$ and $m_{\mathrm{B}^0_\mathrm{d}}$ are the B^0_s and B^0_d masses, as the ratio of decay constants for B^0_d and B^0_s mesons is much better known than the absolute values [2, 3].

CP violation has so far been observed only in the K^0 system, but it is also expected to occur in the B^0 system. Predictions for $\mathrm{Re}\,\epsilon_\mathrm{B}$ are of the order of 10^{-3} in the Standard Model for the B^0_d system [4], and up to an order of magnitude larger in the superweak model [5]. The analogous parameter for the B^0_s system, $\mathrm{Re}\,\epsilon_{\mathrm{B}^0_\mathrm{s}}$, is expected to be smaller by at least an order of magnitude, because $\mathrm{Im}\,V_\mathrm{ts} \approx \lambda \cdot \mathrm{Im}\,V_\mathrm{td}$, where λ comes from the Wolfenstein parametrisation of the CKM matrix [6]. CPT violation may occur in certain string description models of fundamental particles [8]. Although CPT conservation has been tested with high precision in the K^0 system [7], CPT violating effects could be larger in the B system [1, 9].

[1] We use B^0 to refer to either of the neutral B mesons, B^0_d and B^0_s.

The study presented in this paper uses inclusive lepton events, where the identified lepton serves both to select $Z \to b\overline{b}$ events and to determine the flavour of the parent b hadron at decay. The production flavour of this b hadron is determined using a jet charge technique. A vertex finding algorithm is used to estimate the decay length of the b hadron, and a separate algorithm is used to estimate the energy of the hadron, allowing the decay proper time to be calculated. The study of Δm_d and Δm_s is performed neglecting possible CP or CPT violation. Results on $\mathrm{Re}\,\epsilon_B$ and $\mathrm{Im}\,\delta_B$ for the B_d^0 system are then obtained, assuming a negligible CP violating contribution from B_s^0 decays.

2 The OPAL Detector

The OPAL detector has been described elsewhere [10, 11]. Tracking of charged particles is performed by a central detector, consisting of a silicon microvertex detector, a vertex chamber, a jet chamber and z-chambers.[2] The central detector is positioned inside a solenoid, which provides a uniform magnetic field of 0.435 T. The silicon microvertex detector consists of two layers of silicon strip detectors; the inner layer covers a polar angle range of $|\cos\theta| < 0.83$ and the outer layer covers $|\cos\theta| < 0.77$. This detector provided both ϕ- and z-coordinates for data taken in 1993 and 1994, but ϕ-coordinates only for 1991 and 1992. Only ϕ-coordinate information was used in this analysis. The vertex chamber is a precision drift chamber which covers the range $|\cos\theta| < 0.95$. The jet chamber is a large-volume drift chamber, 4.0 m long and 3.7 m in diameter, providing both tracking and ionisation energy loss ($\mathrm{d}E/\mathrm{d}x$) information. The z-chambers measure the z-coordinate of tracks as they leave the jet chamber in the range $|\cos\theta| < 0.72$. The coil is surrounded by a time-of-flight counter array and a barrel lead-glass electromagnetic calorimeter with a presampler. Including the endcap electromagnetic calorimeters, the lead-glass blocks cover the range $|\cos\theta| < 0.98$. The magnet return yoke is instrumented with streamer tubes and serves as a hadron calorimeter. Outside the hadron calorimeter are muon chambers, which cover 93% of the full solid angle.

3 Event simulation

Monte Carlo events are used to predict the relative abundances and decay time distributions for lepton candidates from various physics processes. The JETSET 7.4 Monte Carlo program [12] with parameters tuned to OPAL data [13] was used to generate $Z^0 \to q\overline{q}$ events which were subsequently processed by the detector simulation program [14]. In this version, branching fractions of heavy hadron decays were revised better to reflect measured results [15]. The fragmentation of b and c quarks was parametrised using the fragmentation function of Peterson *et al.* [16], with $\langle x_E \rangle$ for weakly-decaying b and c hadrons given by the central values in Table 1.

Standard Model values of the partial widths of the Z^0 into $q\overline{q}$ were used [20]. The mixture of c hadrons produced both in $Z^0 \to c\overline{c}$ events and in b-hadron decays was as prescribed in

[2] The coordinate system is defined with positive z along the e^- beam direction, θ and ϕ being the polar and azimuthal angles. The origin is taken to be the centre of the detector.

Quantity	Value
$\langle x_E \rangle_{\mathrm{b}}$	0.701 ± 0.008 [17]
$\langle x_E \rangle_{\mathrm{c}}$	0.51 ± 0.02 [18]
$B(\mathrm{b} \to \ell)$	$(10.5 \pm 0.6 \pm 0.5)\%$ [19]
$B(\mathrm{b} \to \mathrm{c} \to \ell)$	$(7.7 \pm 0.4 \pm 0.7)\%$ [19]
$B(\mathrm{b} \to \bar{\mathrm{c}} \to \ell)$	$(1.3 \pm 0.5)\%$ [12, 19]

Table 1: The parameters used for the Monte Carlo simulation. The uncertainties quoted represent the measurement errors, as found in the quoted references.

reference [18]. The semileptonic branching ratios of charm hadrons and associated uncertainties were also those of reference [18]. The central values in Table 1 were taken for the inclusive branching ratios for $\mathrm{b} \to \ell$, $\mathrm{b} \to \mathrm{c} \to \ell$ and $\mathrm{b} \to \bar{\mathrm{c}} \to \ell$. The models used in describing the semileptonic decays of b and c hadrons were those used in determining the central values in reference [18]. Both B^{**} and D^{**} production were included in the simulation, with production rates of 36% of inclusive B and D meson production. Although the measured values quoted in Table 1 are not in all cases the most recent, the differences are not significant for this analysis.

Track impact parameter resolutions were degraded to bring the distributions into agreement with data, as described previously [21].

4 Event selection

The analysis was performed on data collected in the vicinity of the Z^0 peak from 1991 to 1994. Hadronic Z^0 decays were selected using criteria described in a previous publication [22]. For this analysis, events were rejected if the silicon microvertex detector was not operational, resulting in a sample of about 3.0 million events. Tracks and electromagnetic clusters not associated to tracks were grouped into jets using a cone jet algorithm [23]. The size of the cone was chosen so as to include nearly all the decay products of a b hadron into one jet. The jets also include some particles produced in the fragmentation process, which originate directly from the $\mathrm{e}^+\mathrm{e}^-$ collision point.

Electrons and muons with $p > 2$ GeV/c were identified as described in reference [24]. A sample enriched in semileptonic decays of b hadrons was selected by requiring $\alpha_{\mathrm{kin}} > 0.7$, where α_{kin} is the output of a neural network based on kinematic variables [24]. The inputs to this network were p, p_t and a measure of the energy around the lepton, where p_t is the transverse momentum relative to the jet axis (calculated including the lepton). The only difference compared to the previous paper [24] is that the requirement $|\cos\theta| < 0.9$ was removed. Of the final event sample, just over 3% of the leptons have $|\cos\theta| > 0.9$, ranging up to $|\cos\theta| = 0.96$.

For each lepton, an estimated proper decay time was reconstructed for the supposed parent b-hadron as described previously [24]. To summarise, a secondary vertex is reconstructed in the $x - y$ plane using an algorithm to combine tracks with the lepton track. The algorithm was able to form secondary vertices for 70% of the lepton candidates; the remaining 30% were discarded. A decay length is reconstructed by fitting to the reconstructed primary and secondary vertex positions, using the jet axis as a direction constraint. The 3-dimensional

decay length is calculated by dividing the 2-dimensional decay length, L_{xy}, by the $\sin\theta$ of the jet axis. The energy of the b hadron is estimated by first reconstructing the energy of the jet that includes the lepton, using the Z^0 mass to constrain the event kinematics, and then subtracting an estimated contribution from fragmentation particles. The fragmentation particles were separated from the b-hadron decay products using momentum, angle and vertex information. The proper time, t, is formed from the (3-dimensional) decay length L and boost [3]:

$$t = \frac{L}{\beta\gamma} = \frac{m_B}{\sqrt{E_B^2 - m_B^2}} L \; . \tag{4}$$

In this analysis, use is also made of the estimated uncertainty, σ_t, on the proper time, calculated from the separately estimated uncertainties on the decay length, σ_L, and the boost factor, $\sigma_{\beta\gamma}$:

$$\left(\frac{\sigma_t}{t}\right)^2 = \left(\frac{\sigma_L}{L}\right)^2 + \left(\frac{\sigma_{\beta\gamma}}{\beta\gamma}\right)^2 \; , \tag{5}$$

where correlations between the uncertainties on L and $\beta\gamma$ are neglected. This is unimportant because the shape of the t distribution is parametrised from Monte Carlo, as discussed in the next section. The use of σ_t, estimated event by event, improves the sensitivity of the analysis since only events with small σ_t can discriminate between large oscillation frequencies. For each event, an initial estimate of σ_L is calculated from the error matrices of the tracks assigned to the secondary vertex. Monte Carlo studies showed that the decay length resolution worsens as the total momentum of tracks assigned to the vertex (excluding the lepton) decreases. These studies also showed that the resolution worsens with increasing L_{xy}. Both effects result from the inclusion in the secondary vertex of tracks that do not originate from the decay of the b hadron or its daughters, i.e. fragmentation products. Neither of these effects is fully described by the initial estimate of σ_L. Corrections were therefore applied to σ_L based on parametrisations of the Monte Carlo predictions. Monte Carlo studies of the b-hadron energy estimate showed that the resolution depends strongly on L_{xy} and the fragmentation energy in the jet. The uncertainty $\sigma_{\beta\gamma}$ was estimated by parametrising the dependence on these two quantities predicted by the Monte Carlo. The performance of the proper time reconstruction is shown in Figure 1 for Monte Carlo events, and the distribution of σ_t is shown in Figure 2.

For each event, the b-hadron flavour at production was tagged using the jet charge technique described in a previous paper [25]. The jet charge was defined as

$$Q_{jet} = \sum q_i \left(\frac{p_i^l}{E_{\rm beam}}\right)^\kappa \; , \tag{6}$$

where q_i, p_i^l are the charge and longitudinal momentum component (along the jet direction) of track i, $E_{\rm beam}$ is the beam energy, and the sum is over all tracks in the jet. The jet charge was formed for two jets: the jet containing the lepton and the highest energy jet that did not contain the lepton, with κ chosen to be 0 and 1 respectively. These two values of jet charge were combined into a single value,

$$Q_{2jet} = Q_{jet}^{\kappa=0}(\ell) - 10 \times Q_{jet}^{\kappa=1}(\mathrm{opp}) \; , \tag{7}$$

where ℓ denotes the lepton jet, and 'opp' denotes the other jet. The factor of 10 was chosen to give a charge separation between produced b and $\bar{\rm b}$ hadrons that is close to optimal [25].

[3] We use the notation $\hbar = c = 1$.

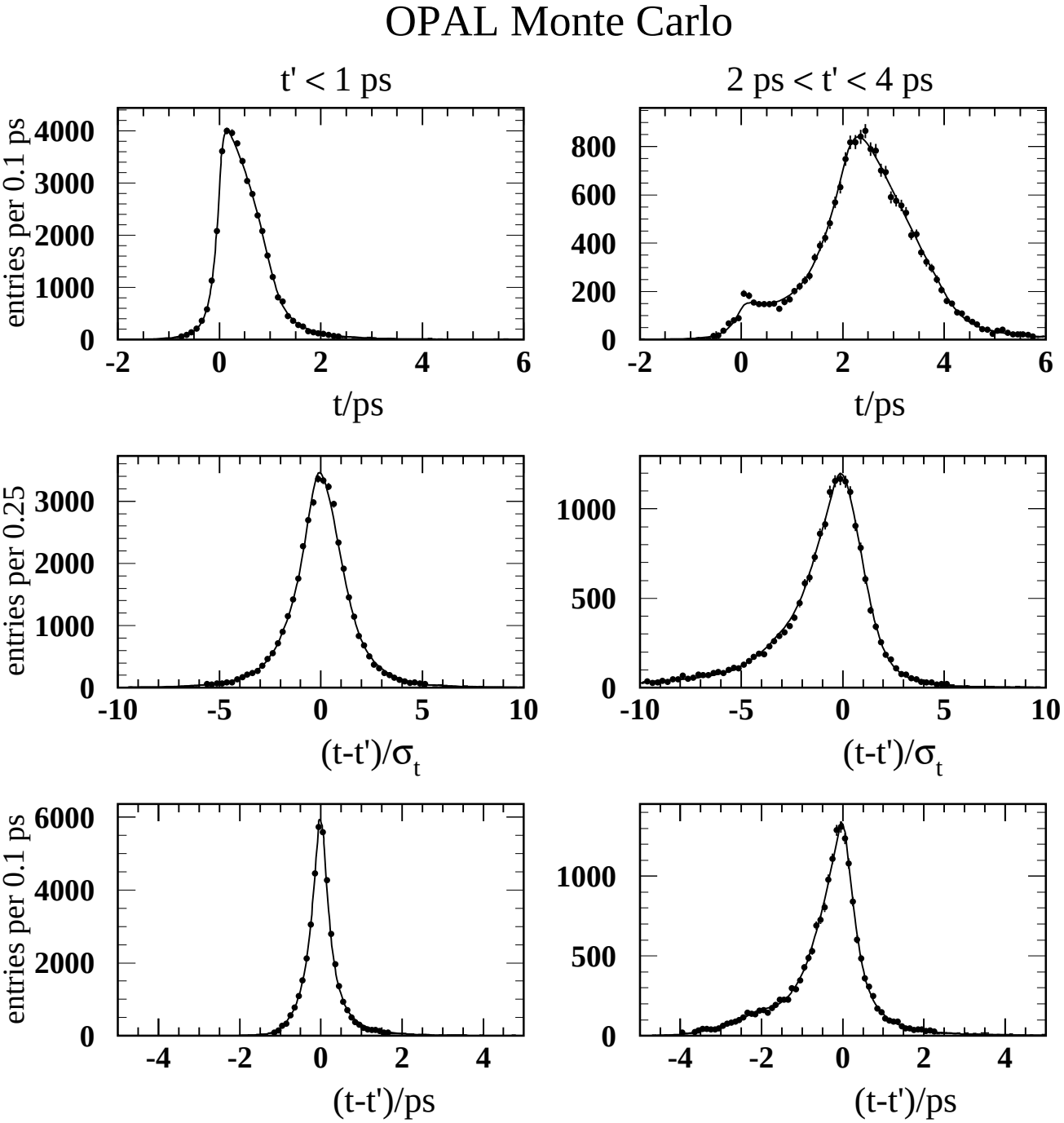

Figure 1: Distributions of t, $(t-t')/\sigma_t$ and $t-t'$ for semileptonic decays of b hadrons in two ranges of true decay proper times: $t' < 1$ ps and 2 ps $< t' <$ 4 ps. The points represent the Monte Carlo simulation, and the curves represent the parametrisation.

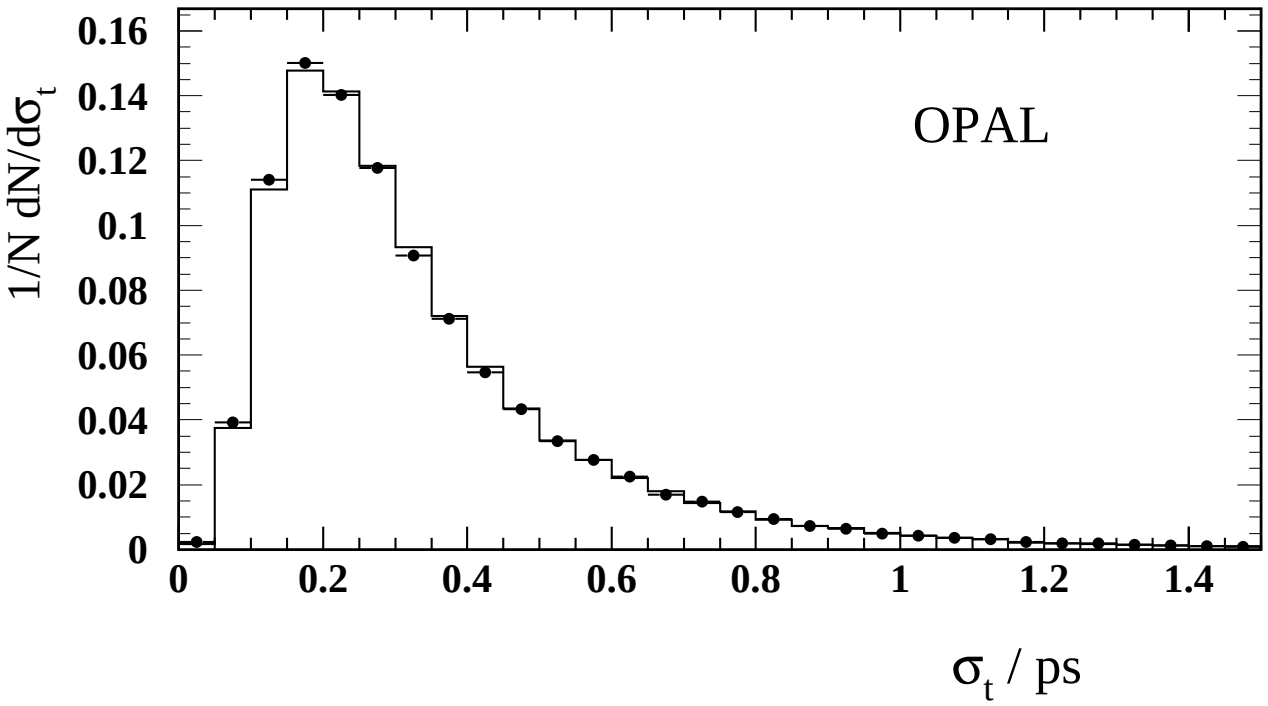

Figure 2: Distribution of σ_t. The points represent the data, and the line the Monte Carlo prediction.

If more than one lepton was selected in a given event, only the one with the highest value of $(\frac{p}{10.})^2 + p_t^2$ was retained, where p is in GeV/c. A total of 94 843 events remain after all selection criteria, where about 75% of the lepton candidates are expected to originate from semileptonic decays of b hadrons.

5 Likelihood function

The results obtained in this paper are extracted using a maximum likelihood fitting procedure, where the overall likelihood is the product of the likelihoods calculated for each event. In order to construct the likelihood function, the contributions to the selected lepton candidates were split into 11 sources:

1. lepton candidates from light quark events ($\mathrm{Z} \to \mathrm{u\overline{u}}$, $\mathrm{d\overline{d}}$ and $\mathrm{s\overline{s}}$);
2. leptons from semileptonic decays of c hadrons in $\mathrm{Z} \to \mathrm{c\overline{c}}$ events;
3. lepton candidates in $\mathrm{Z} \to \mathrm{c\overline{c}}$ events not from semileptonic decays of c hadrons;
4. lepton candidates in $\mathrm{Z} \to \mathrm{b\overline{b}}$ events that do not originate from a b hadron or its daughters;
5. lepton candidates in $\mathrm{Z} \to \mathrm{b\overline{b}}$ events that do not come from semileptonic decays of b hadrons or c hadrons, but do originate from a b hadron or its daughters;
6. leptons from $\mathrm{b} \to \mathrm{c} \to \ell$ decays originating from $\mathrm{B^0_d}$ decays;

7. leptons from $b \to c \to \ell$ decays originating from B_s^0 decays;
8. leptons from $b \to c \to \ell$ decays originating from B^+ or b-baryon decays;
9. leptons from semileptonic B_d^0 decays;
10. leptons from semileptonic B_s^0 decays;
11. leptons from semileptonic B^+ or b-baryon decays.

Note that the notation $b \to c \to \ell$ used here excludes decays of the type $b \to \bar{c} \to \ell$, where the b refers to the quark that decays, after any mixing has occurred. The last three sources are taken also to include decays of the type $b \to \bar{c} \to \ell$ as well as $b \to \tau \to \ell$. Note also that decays of the type $b \to J/\psi \to \ell$ are classed either as $b \to c \to \ell$ or semileptonic b hadron decays depending on the charge correlation of the lepton and the b quark. The predicted fraction of the overall sample contributed by each source is indicated in Table 2. The statistical errors on these numbers are not important.

Source	1	2	3	4	5	6	7	8	9	10	11
Fraction	0.063	0.089	0.011	0.005	0.013	0.025	0.005	0.025	0.299	0.089	0.377

Table 2: The predicted fraction of the overall selected sample due to each source.

The joint distribution of t and σ_t is of the form

$$\mathcal{T}_{ij}(t,\sigma_t) = \int \mathcal{S}_i(\sigma_t|t')\mathcal{R}_i(t|\sigma_t,t')\mathcal{P}_{ij}(t')\mathcal{E}_i(t')\mathrm{d}t' \tag{8}$$

where t' is the true proper decay time for a given source, $\mathcal{P}$ is the physics function, $\mathcal{E}$ is an efficiency function, $\mathcal{R}$ is the resolution function for given values of t' and σ_t, and $\mathcal{S}$ gives the distribution of σ_t for a given t'. The subscript i represents the source number (1 to 11). When CP violation is neglected, the subscript j is 2 for leptons from decays of B mesons that decayed as the antiparticle of the meson produced (mixed), or 1 otherwise. Note that the physics function describes the evolution of each source as a function of the true proper decay time. For sources 1, 3 and 4, $\mathcal{P}$ is taken to be a delta function at $t' = 0$. Any true lifetime content in these sources is absorbed by the resolution function. For source 2, t' represents the proper decay time of the c hadron, but for all the other sources t' represents the proper decay time of the b hadron. Sources 6,7,9 and 10 are divided into two components: unmixed ($j = 1$) and mixed ($j = 2$). For these components:

$$\mathcal{P}_{i1} = \frac{\exp(-\frac{t'}{\tau_i})}{\tau_i} \cdot \frac{1+\cos\Delta m_q t'}{2}\,, \quad \mathcal{P}_{i2} = \frac{\exp(-\frac{t'}{\tau_i})}{\tau_i} \cdot \frac{1-\cos\Delta m_q t'}{2}\,, \tag{9}$$

where $\Delta m_q = \Delta m_d$ (Δm_s), and $\tau_i = \tau_{B_d^0}$ ($\tau_{B_s^0}$) for sources 6 and 9 (7 and 10). When considering possible CP and CPT violation, sources 6 and 9 (B_d^0) were divided into four components according to the flavour of the B at production and decay [9] :

$$B_d^0 \to B_d^0 \;:\; \mathcal{P}_{i1} = \frac{\exp(-\frac{t'}{\tau_i})}{\tau_i} \cdot \frac{1+\cos\Delta m_d t' - 4\mathrm{Im}\,\delta_B \sin\Delta m_d t'}{2k_B}$$

$$
\begin{aligned}
\mathrm{B^0_d} \to \bar{\mathrm{B}}^0_\mathrm{d} \;:\; \mathcal{P}_{i2} &= \frac{\exp(-\frac{t'}{\tau_i})}{\tau_i} \cdot \frac{1-\cos\Delta m_\mathrm{d} t'}{2} \cdot \frac{1-4\mathrm{Re}\,\epsilon_\mathrm{B}}{k_\mathrm{B}} \\
\bar{\mathrm{B}}^0_\mathrm{d} \to \bar{\mathrm{B}}^0_\mathrm{d} \;:\; \mathcal{P}_{i3} &= \frac{\exp(-\frac{t'}{\tau_i})}{\tau_i} \cdot \frac{1+\cos\Delta m_\mathrm{d} t' + 4\mathrm{Im}\,\delta_\mathrm{B} \sin\Delta m_\mathrm{d} t'}{2k_{\bar{\mathrm{B}}}} \\
\bar{\mathrm{B}}^0_\mathrm{d} \to \mathrm{B^0_d} \;:\; \mathcal{P}_{i4} &= \frac{\exp(-\frac{t'}{\tau_i})}{\tau_i} \cdot \frac{1-\cos\Delta m_\mathrm{d} t'}{2} \cdot \frac{1+4\mathrm{Re}\,\epsilon_\mathrm{B}}{k_{\bar{\mathrm{B}}}}
\end{aligned}
\tag{10}
$$

where k_B is a constant which ensures the normalisation $\int(\mathcal{P}_{i1}+\mathcal{P}_{i2})\mathrm{d}t' = 1$, and similarly for $k_{\bar{\mathrm{B}}}$ and $\mathcal{P}_{i3}+\mathcal{P}_{i4}$. Note that CP and CPT violation in the $\mathrm{B^0_s}$ system is neglected in this analysis. Sources 8 and 11 were described by a double exponential, with the lifetime parameters corresponding to the $\mathrm{B^+}$ and b-baryon lifetimes. Source 2 was also parametrised by a double exponential to describe the different individual lifetimes of the c hadrons. This approximation gave a good description of this background in the Monte Carlo.

The function $\mathcal{E}$ describes the efficiency for reconstructing a proper decay time as a function of t'. A single function was common for sources 9,10,11, a second function was common for sources 6,7,8, and individual functions were used for sources 2 and 5. For sources 9,10,11, the efficiency is about 5% smaller at $t' = 0$ ps than at $t' = 1.5$ ps, above which point it is flat.

The functions $\mathcal{S}$ and $\mathcal{R}$ were parametrised using Monte Carlo events. For this purpose, one set of functions was common to sources 5,9,10,11, and another set was common to sources 6,7,8. The effects of leptons from secondary decays ($\mathrm{b} \to \mathrm{c} \to \ell$, $\mathrm{b} \to \bar{\mathrm{c}} \to \ell$, $\mathrm{b} \to \tau \to \ell$) are taken into account in the resolution functions, rather than the physics functions. Distributions of t, $t - t'$ and $(t - t')/\sigma_t$ for semileptonic decays of b hadrons are shown in Figure 1 for two ranges of t'. These are compared to the resolution function $\mathcal{R}$ integrated over the relevant proper time interval, and also over σ_t. The distribution of σ_t is shown for data and Monte Carlo in Figure 2, equivalent to $\mathcal{S}$ integrated over t' and averaged over all sources. The Monte Carlo describes the data well, and it is clear that some events are measured much better than others.

The normalisation of the joint distribution function $\mathcal{T}$ for each source is determined by

$$
\int \sum_j \mathcal{P}_{ij}(t')\mathcal{E}_i(t')\mathrm{d}t' = 1\;, \quad \int \mathcal{R}_i(t|\sigma_t, t')\mathrm{d}t = 1\;, \quad \int \mathcal{S}_i(\sigma_t|t')\mathrm{d}\sigma_t = 1\;. \tag{11}
$$

For sources involving mixing, the normalisation condition for $\mathcal{P}$ applies to the sum over mixed and unmixed functions.

To describe the charge distributions for each source, we first define the fraction of each source, ξ_{ij}, for which the lepton has the same charge sign as the quark, at its production, that produced the lepton jet. For example ξ is 1 for semileptonic decays of b hadrons, but 0 for $\mathrm{b} \to \mathrm{c} \to \ell$ decays when no mixing has occurred in either case. The full set of values for ξ is given in Table 3, where the values for sources 1,3,4 and 5 are taken from the Monte Carlo simulation. Variation of these values was found to lead to negligible changes in the results of this paper. The sign of the jet charge, Q_{2jet}, is an estimate of the charge sign of the quark, before any mixing, that produced the lepton jet. The quantity $\eta_{ij}(|Q_{2jet}|)$ is defined as the probability that these charge signs disagree, where i represents the source number and $j = 1$ or 2 (also 3 or 4 when considering CP(T) violation as in equation 10) to represent no mixing or mixing, respectively, in the lepton jet. Monte Carlo events were used to parametrise η as a

function of $|Q_{2jet}|$. For sources from $Z \to b\overline{b}$ events, i.e. sources 4 to 11, the effect of mixing in the jet that does not contain the lepton was taken into account by modifying η as a function of χ, the time-averaged mixing parameter, averaged over all b hadron species weighted by their production fractions in Z^0 decays:

$$\eta_{ij}^{\chi} = \eta_{ij}^{\chi=0} \cdot (1 - X) + (1 - \eta_{ij}^{\chi=0}) \cdot X \ , \quad \text{where} \quad X = \chi \cdot w(|Q_{2jet}|) \ , \tag{12}$$

and the weighting function $w(|Q_{2jet}|)$ was parametrised from Monte Carlo data. Note that χ is computed in the fit from $\Delta m_{\rm d}$, $\Delta m_{\rm s}$, the lifetimes and the fractions of $B_{\rm d}^0$ and $B_{\rm s}^0$ mesons produced. To describe the charge distribution for each source, we define

$$\mathcal{Q}_{ij} = \begin{cases} \xi_{ij} \cdot (1 - \eta_{ij}) + (1 - \xi_{ij}) \cdot \eta_{ij} & \text{if } Q_\ell Q_{2jet} > 0 \\ (1 - \xi_{ij}) \cdot (1 - \eta_{ij}) + \xi_{ij}\eta_{ij} & \text{otherwise} \end{cases} \ , \tag{13}$$

where Q_ℓ is the charge of the lepton candidate. The function $\mathcal{Q}_{ij}$ represents the probabilities for finding $Q_\ell Q_{2jet}$ positive or negative for a given $|Q_{2jet}|$. A comparison of the distribution of $Q_\ell Q_{2jet}$ between data and Monte Carlo is shown in Figure 3, where the Monte Carlo distribution assumed $\Delta m_{\rm d} = 0.45$ ps^{-1} and $\Delta m_{\rm s} = 15$ ps^{-1}. A reasonable agreement is observed. The distributions of $Q_\ell Q_{2jet}$ for semileptonic decays of neutral B mesons that have and have not mixed are compared in Figure 4. For neutral unmixed B mesons, η is about 0.3 for $|Q_{2jet}| = 2$. When considering CP(T) violation, two out of the four physics functions defined in equation 10 are used for a particular source, according to the lepton charge. For example, for a negatively charged lepton, the functions corresponding to $j = 1$ and $j = 4$ would be used for source 8.

Source		1	2	3	4	5	6	7	8	9	10	11
ξ	unmixed	0.69	1	0.62	0.67	0.67	0	0	0	1	1	1
	mixed						1	1		0	0	

Table 3: Values of ξ for each source. The second row represents the case of leptons from B mesons that have mixed.

The final ingredient to the likelihood is the fraction of each source, which is estimated event by event based on the value of the neural net output, $\alpha_{\rm kin}$, with a small correction for the absolute value of the jet charge, $|Q_{2jet}|$, giving

$$\mathcal{N}_i(\alpha_{\rm kin}, |Q_{2jet}|) = \frac{\mathcal{A}_i(\alpha_{\rm kin})\mathcal{B}_i(|Q_{2jet}|)}{\sum_i \mathcal{A}_i(\alpha_{\rm kin})\mathcal{B}_i(|Q_{2jet}|)} \ . \tag{14}$$

The function $\mathcal{A}_i$ is the fraction of events due to source i for a given value of $\alpha_{\rm kin}$, and $\mathcal{B}_i$ describes the distribution $|Q_{2jet}|$ for source i. Note that different sources give rise to slightly different distributions of $|Q_{2jet}|$, in particular light quark events give rise to larger values of $|Q_{2jet}|$ than do $b\overline{b}$ events on average. The correction, using the function $\mathcal{B}_i$, takes this into account. Sources 9, 10 and 11 give rise to very similar distributions of $|Q_{2jet}|$, and are described by a common function $\mathcal{B}$. The function $\mathcal{A}_i(\alpha_{\rm kin})$ is parametrised from Monte Carlo events, taking into account the recipe for modelling the momentum spectra of leptons in the rest frame for the semileptonic decays of b and c hadrons and for $b \to c \to \ell$ decays described in a previous paper [18]. The predicted distribution of $\alpha_{\rm kin}$ is compared to the data in Figure 5, where the contribution of events from semileptonic decays of b hadrons is also indicated. Note that the semileptonic branching ratios of the individual b hadrons were assumed to be proportional to the lifetimes.

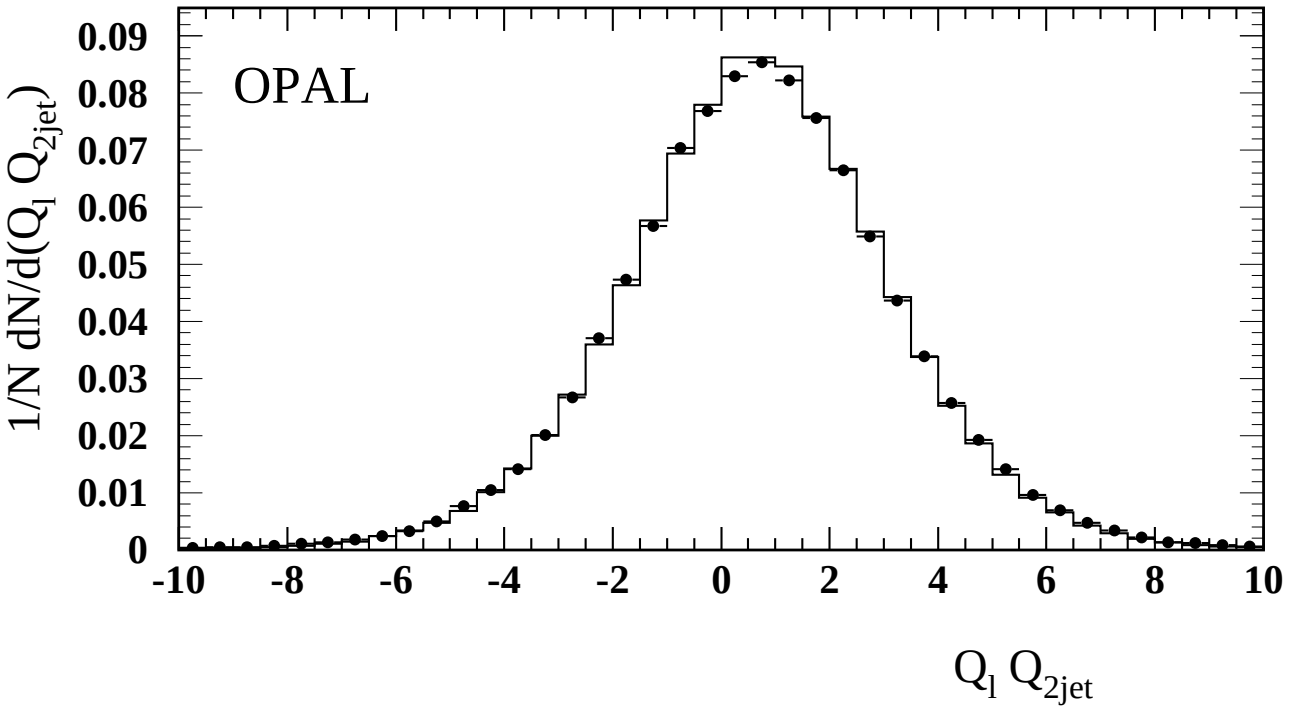

Figure 3: The distribution of $Q_\ell Q_{2jet}$ for data is shown by the points with error bars. The curve indicates the Monte Carlo prediction, assuming $\Delta m_{\rm d} = 0.45$ ps^{-1} and $\Delta m_{\rm s} = 15$ ps^{-1}.

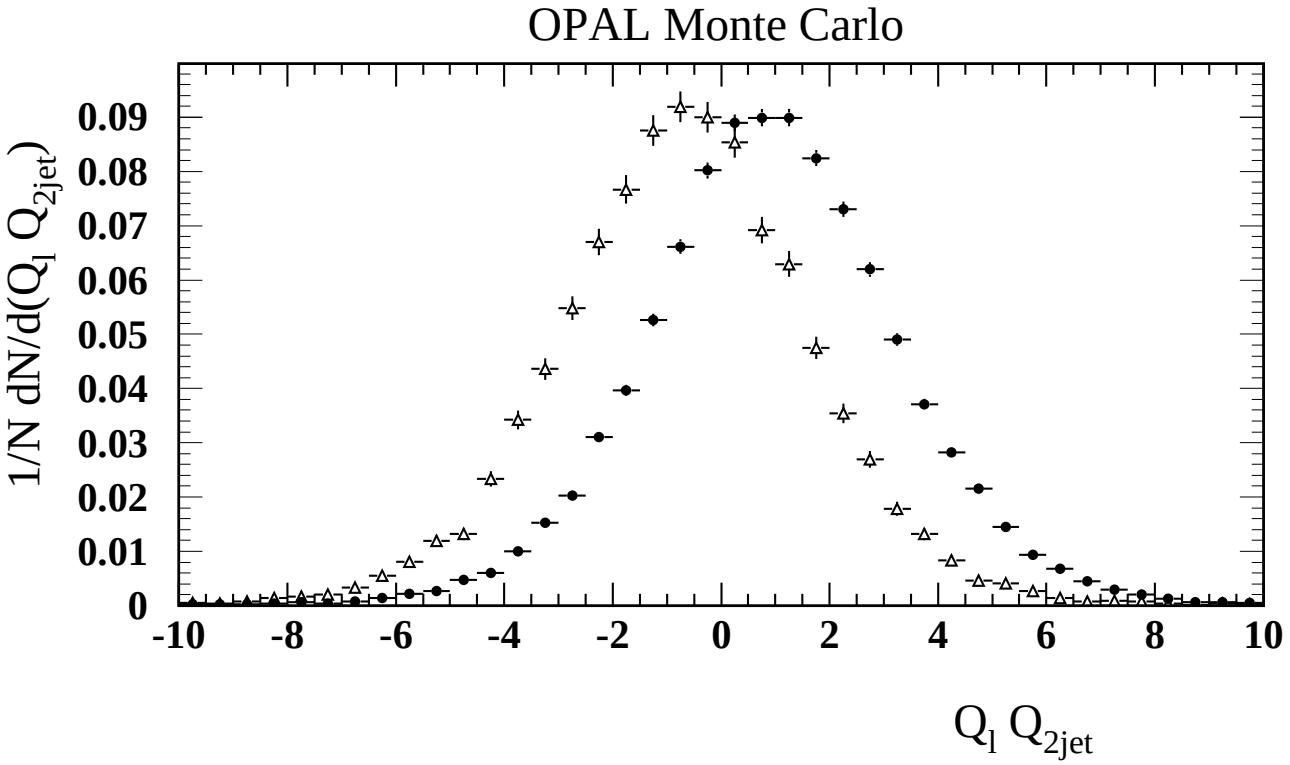

Figure 4: The distribution of $Q_\ell Q_{2jet}$ for semileptonic decays of neutral B mesons in the Monte Carlo. The solid points represent unmixed B mesons while the triangles show the distribution for mixed B mesons.

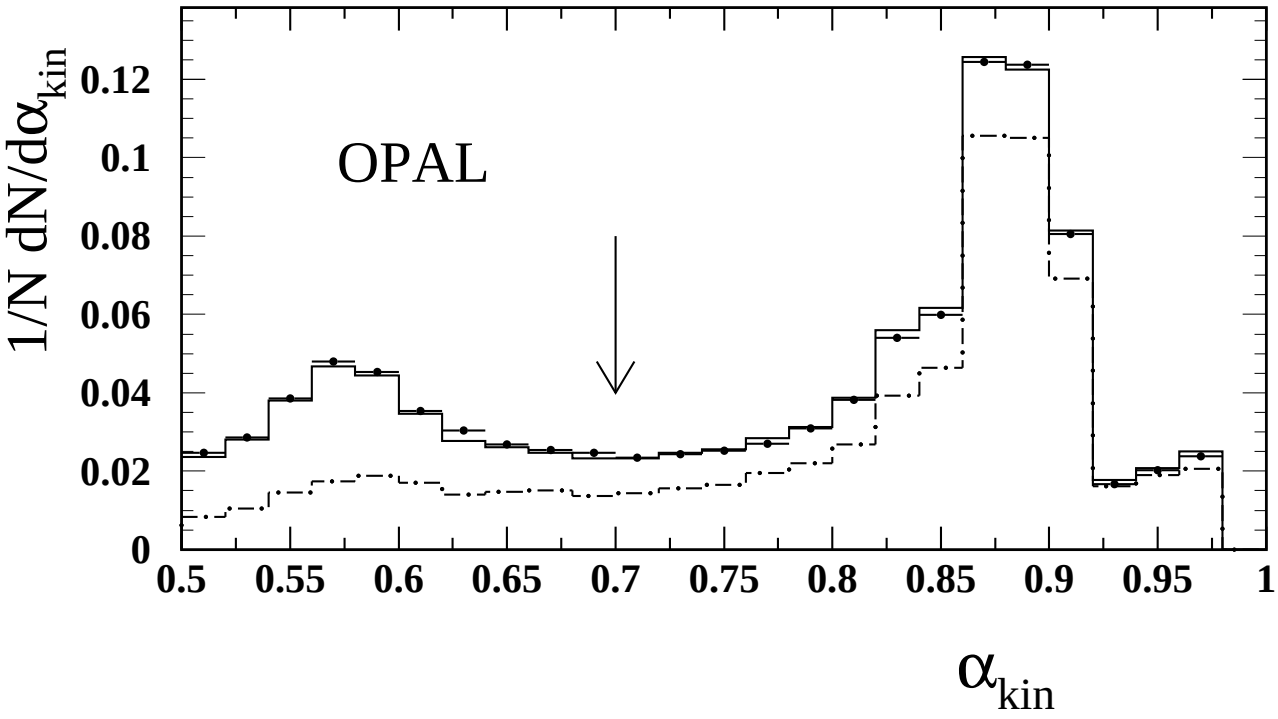

Figure 5: The distribution of $\alpha_{\rm kin}$ for data is shown by the points. The solid histogram shows the Monte Carlo prediction, and the dashed-dotted histogram shows the contribution from semileptonic decays of b hadrons. The arrow indicates the selection cut; events to the left of the arrow were rejected.

The overall likelihood of the event sample is taken as

$$\mathcal{L}_{\rm data} = \prod_{m=1}^{n} \sum_{i,j} \mathcal{T}_{ij}(t^m, \sigma_t^m) \mathcal{Q}_{ij}(Q_\ell^m Q_{2jet}^m) \mathcal{N}_i(\alpha_{\rm kin}^m, |Q_{2jet}^m|) \ , \tag{15}$$

where the product is over all the events in the sample.

6 Results

In order to obtain information about $\Delta m_{\rm d}$ and $\Delta m_{\rm s}$, the likelihood, $\mathcal{L}$, was maximised with respect to $\Delta m_{\rm d}$ for many values of $\Delta m_{\rm s}$. However, in order to include systematic uncertainties, other parameters in the likelihood calculation were also allowed to vary, but under Gaussian constraints, i.e.

$$\mathcal{L} = \mathcal{L}_{\rm data} \times \mathcal{L}_{\rm constr} \tag{16}$$

where $\mathcal{L}_{\rm constr}$ is the product of the Gaussian constraints. Thus a multiparameter fit was performed for each $\Delta m_{\rm s}$ point. This procedure was also employed in reference [24]. The parameters that were allowed to vary and the constraints on these parameters are listed in Table 4. In this table, $f_{\rm s}$ is defined as the production fraction $f({\rm b} \to {\rm B_s^0})$. The value is constrained both by direct measurements, giving a rate of $(11.1 \pm 2.6)\%$ [15] relative to all weakly decaying b hadrons, and by the measured average mixing rate of b hadrons, $\chi = 0.126 \pm 0.008$ [15] together

Parameter	Constraint
$f_{\rm s}$	see text
$f_{\rm baryon}$	$(13.2 \pm 4.1)\%$
$f_{\rm b\to c\to\ell}$	$\pm 15\%$ × nominal
$f_{\rm c}$	$\pm 20\%$ × nominal
$f_{\rm uds}$	$\pm 20\%$ × nominal
$\langle\tau_{\rm b}\rangle$	1.549 ± 0.020 ps
$\tau^+/\tau_{\rm d}$	1.03 ± 0.06
$\tau_{\rm s}/\tau_{\rm d}$	1.03 ± 0.075
$\tau_{\Lambda_{\rm b}}/\tau_{\rm d}$	0.73 ± 0.06
$\delta Q_{\rm b}$	0 ± 0.06
$\delta Q_{\rm mix}$	0 ± 0.06
$\delta Q_{\rm B^+}$	0 ± 0.06
$\delta Q_{\rm udsc}$	0 ± 0.06
$f_{\rm D^{**}}$	$(35 \pm 10)\%$

Table 4: Constrained parameters in the fit

with knowledge of the equivalent parameters, $\chi_{\rm d(s)}$, for $\rm B^0_d(B^0_s)$ mesons and the fraction of b baryons, where

$$\chi_{\rm d} = \frac{1}{2}\left(\frac{x_{\rm d}^2}{1+x_{\rm d}^2}\right) \ , \quad x_{\rm d} = \Delta m_{\rm d}\tau_{\rm d} \ , \tag{17}$$

with $\tau_{\rm d}$ representing the $\rm B^0_d$ lifetime, and similarly for $\chi_{\rm s}$. This is equivalent to the constraint $f_{\rm s} = (11.2^{+1.8}_{-1.9})\%$ [15] except that the values of $\chi_{\rm d}$ and $\chi_{\rm s}$ are calculated from the values of $\Delta m_{\rm d}$ and $\Delta m_{\rm s}$ in the fit, together with the appropriate lifetimes, and $f_{\rm baryon}$, defined as $f(\rm b \to b\ baryon)$, is also taken from the value in the fit. The quoted constraint on $f_{\rm baryon}$ is taken from reference [15]. When varying $f_{\rm s}$ and $f_{\rm baryon}$, the following rules are applied:

$$f_{\rm d} + f_{\rm u} + f_{\rm s} + f_{\rm baryon} = 1 \ \text{ and } \ f_{\rm d} = f_{\rm u} \ , \tag{18}$$

where $f_{\rm d}$ and $f_{\rm u}$ are the equivalent production fractions for $\rm B^0_d$ and $\rm B^+$ respectively. The actual fraction of selected leptons coming from $\rm B^0_s$ mesons (b baryons) is also affected by the semileptonic branching ratio, which is assumed to be proportional to the ratio of lifetimes $\tau_{\rm s}/\langle\tau_{\rm b}\rangle$ ($\tau_{\Lambda_{\rm b}}/\langle\tau_{\rm b}\rangle$), where $\tau_{\rm s}$ is the $\rm B^0_s$ lifetime, $\tau_{\Lambda_{\rm b}}$ the average lifetime for b baryons and $\langle\tau_{\rm b}\rangle$ is the average lifetime for b hadrons. Similarly, the fraction of selected leptons coming from $\rm B^+$ relative to $\rm B^0_d$ decays depends on the ratio $\tau^+/\tau_{\rm d}$, where τ^+ is the $\rm B^+$ lifetime. The parameter $f_{\rm b\to c\to\ell}$ is a scaling factor affecting the source fractions for $\rm b \to c \to \ell$ processes, sources 6 to 8. The uncertainty quoted includes uncertainties due to branching fractions, decay modelling and detector simulation. The parameter $f_{\rm c}$ is a scale factor multiplying the source fractions for sources 2 and 3, and $f_{\rm uds}$ is the corresponding parameter for source 1. The uncertainty on $f_{\rm c}$ covers uncertainties due to the charm semileptonic branching ratio, the modelling of the $\alpha_{\rm kin}$ distribution and lepton background. The uncertainty on $f_{\rm uds}$ is due to uncertainties in the lepton background rates. The lifetime constraints indicated in the table were taken from the Particle Data Group review [15]. Note that the existence of two different lifetimes for the $\rm B^0_s$ mass eigenstates is expected to have a negligible effect on this analysis and has been neglected.

The parameter $\delta Q_{\rm b}$ represents an offset to the Monte Carlo distributions of Q_{2jet} for $\mathrm{Z} \to \mathrm{b\overline{b}}$ events before calculation of η_{ij}. Such an offset moves the distributions for produced b and $\overline{\mathrm{b}}$ hadrons closer together or further apart. Thus it causes a change in η as a function of Q_{2jet}, and is equivalent to an uncertainty in η of about ± 0.02 when $\eta = 0.25$. Monte Carlo predictions for η were tested to this level in a previous paper [25]. The parameter $\delta Q_{\rm mix}$ has the same definition as $\delta Q_{\rm b}$, but applies only to events where the lepton originates from a mixed B meson. The parameter $\delta Q_{\rm B^+}$ is also defined in the same way, but applies only to events where the lepton originates from B^+ decays. Similarly, $\delta Q_{\rm udsc}$ applies only to $\mathrm{u\overline{u}}$, $\mathrm{d\overline{d}}$, $\mathrm{s\overline{s}}$ or $\mathrm{c\overline{c}}$ events. The parameter $f_{\rm D^{**}}$ simulates the uncertainty on the rate of $\mathrm{b} \to \mathrm{c} \to \ell$ decays from B^0 and B^+ mesons relative to all b hadrons due to the effect of varying the rate of decays through a D^{**}. A variation in the rate of $\mathrm{b} \to \mathrm{c} \to \ell$ decays from $\mathrm{B}_{\rm s}^0$ mesons relative to all b hadrons was also considered, but found to have a negligible effect.

The uncertainty due to the resolution functions, $\mathcal{R}$ and $\mathcal{S}$, was not taken into account using this technique. Instead, these functions were reparametrised without applying the smearing of the track impact parameters in the Monte Carlo, and the likelihood analysis repeated using the new functions. The effect of fragmentation uncertainties on the resolution functions was assessed by using Monte Carlo events generated with $\langle x_E \rangle_{\rm b}$ shifted by 0.02 relative to the central value. Such a change represents a shift of over 2σ with respect to the measured value [17], but is inflated to include the effect of shape uncertainties. Uncertainty due to charm fragmentation is expected to have a negligible effect, and was neglected.

6.1 Determination of $\Delta m_{\rm d}$

With $\Delta m_{\rm s}$ fixed to 15 ps^{-1} the multiparameter fit was performed, with the result

$$\Delta m_{\rm d} = 0.444 \pm 0.034 \ \mathrm{ps}^{-1} \ .$$

This error includes systematic components, due to the constraints of Table 4, as well as a statistical component. The fitted value of $f_{\rm s}$ was $(10.6 \pm 1.9)\%$, and the calculated value of χ was 0.115. The distribution of t from the fit is superimposed on the data in Figure 6. Shown in Figure 7 is the ratio R versus t for $|Q_{2jet}| > 2$, and $\langle Q_\ell Q_{2jet} \rangle$ versus t for $|Q_{2jet}| < 2$. Here R is defined as the fraction of events that have $Q_\ell Q_{2jet} < 0$. The ratio R is not an appropriate variable to plot for $|Q_{2jet}| < 2$, because η changes rapidly with $|Q_{2jet}|$ in this region and, in particular, many of the events have $|Q_{2jet}|$ close to 0, where there is no sensitivity. The mean value of $Q_\ell Q_{2jet}$ is more sensitive than R in this region. Conversely, since η changes only slowly with Q_{2jet} when $|Q_{2jet}| > 2$, R is the more appropriate variable in this region.

The systematic error on $\Delta m_{\rm d}$ due to tracking resolution was assessed, as described in the previous section, to be ± 0.004 ps^{-1}. The contribution from the b fragmentation uncertainty was found to be ± 0.003 ps^{-1}. The effect of the uncertainty in the fraction of B mesons decaying to D^{**} on the fitted resolution functions was assessed by repeating the analysis using resolution functions determined from a Monte Carlo that did not include D^{**}. The difference between the resulting $\Delta m_{\rm d}$ value and the central value quoted above was divided by 3 to correspond to an uncertainty of $\pm 10\%$ (a relative error of 30%) in the production of D^{**} per B meson. This procedure contributed an uncertainty of ± 0.001 ps^{-1} on $\Delta m_{\rm d}$. The systematic error due to $\Delta m_{\rm s}$ was assessed by taking the largest excursions on the fitted value of $\Delta m_{\rm d}$ when the fit

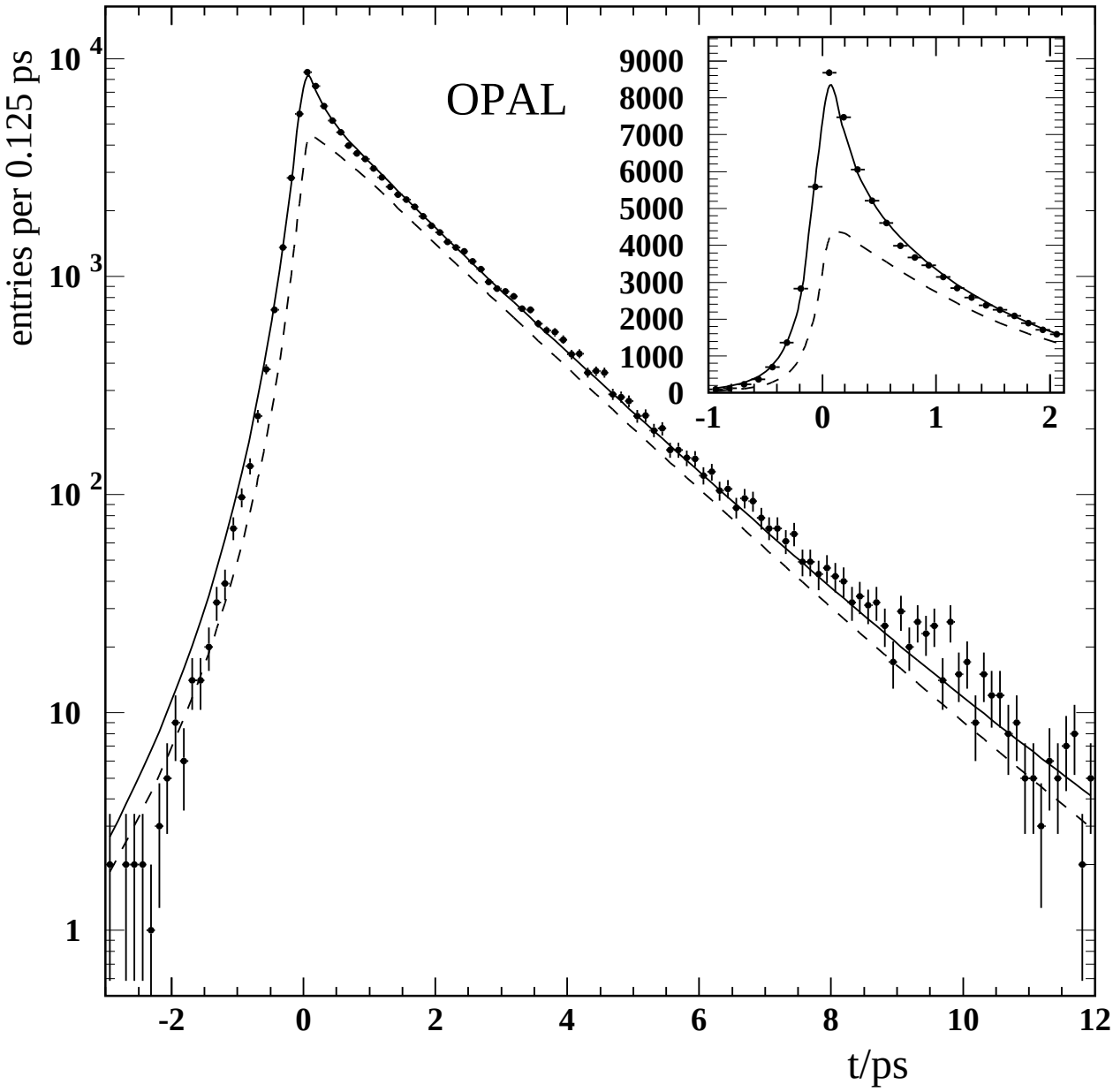

Figure 6: The distribution of t for the selected events in the data. The solid line represents the result of the fit, while the dashed line indicates the component from semileptonic decays of b hadrons, sources 9, 10 and 11. The insert shows the same distribution on a linear scale.

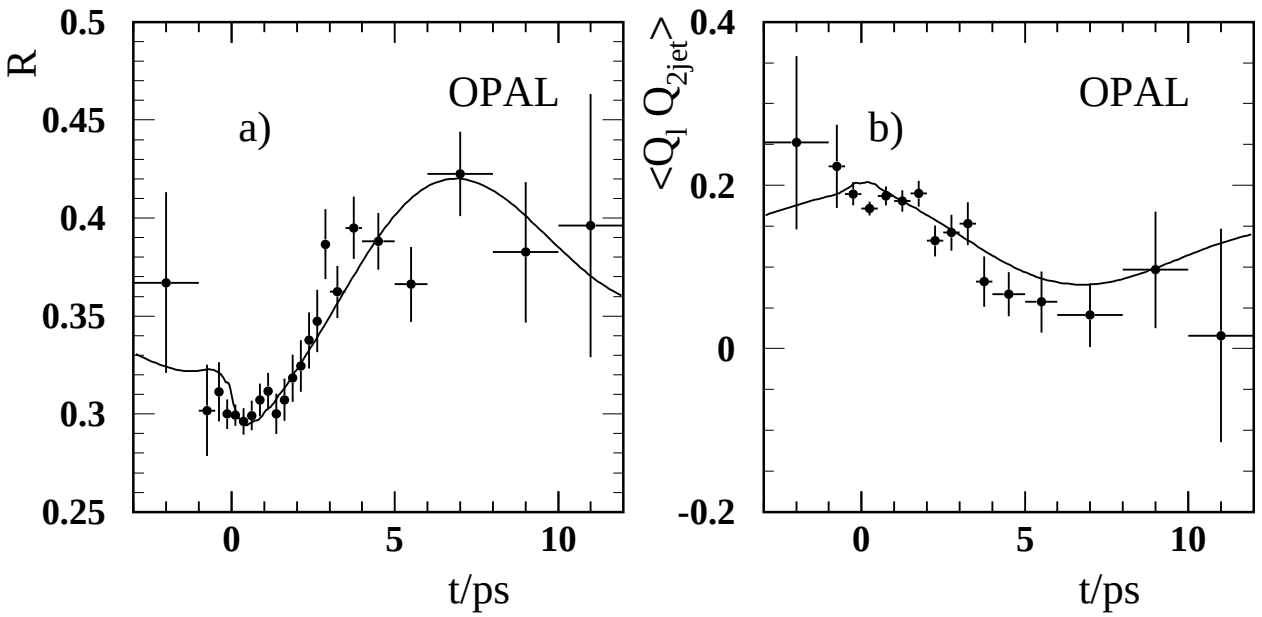

Figure 7: a) The ratio R versus t for data with $|Q_{2jet}| > 2$. b) $\langle Q_\ell Q_{2jet} \rangle$ versus t for data with $|Q_{2jet}| < 2$. The line shows the result of the fit when $\Delta m_{\rm s} = 15$ ps^{-1} in both a) and b).

was repeated for different values of $\Delta m_{\rm s}$ in the range $\Delta m_{\rm s} \geq 6.6$ ps^{-1}. We consider the range $\Delta m_{\rm s} < 6.6$ ps^{-1} to be excluded by previous measurements [24, 26, 27, 29]. The error on $\Delta m_{\rm d}$ from this source was $^{+0.009}_{-0.0002}$ ps^{-1}. The errors on $\Delta m_{\rm d}$ resulting from different ranges of $\Delta m_{\rm s}$ are given in Table 5. The uncertainty due to the weighting function $w(|Q_{2jet}|)$ was found to be negligible.

Lower limit on $\Delta m_{\rm s}$ (ps^{-1})	Systematic uncertainty on $\Delta m_{\rm d}$(ps^{-1})
3	$+0.014 \quad -0.0002$
6.6	$+0.009 \quad -0.0002$
8	$+0.004 \quad -0.0002$
10	$+0.001 \quad -0.0002$

Table 5: The systematic error on $\Delta m_{\rm d}$ resulting from different ranges of $\Delta m_{\rm s}$ values.

The final result for $\Delta m_{\rm d}$ is $\Delta m_{\rm d} = 0.444 \pm 0.034\ ^{+0.011}_{-0.005}$ ps^{-1}, where, as above, the first error has a systematic component. To aid comparison with previous measurements, the systematic components to the fit error (due to the constraints of Table 4) were calculated by determining the effect of changing each constraint by the error given in Table 4, one at a time. The results are shown in Table 6. We can now rewrite the result for $\Delta m_{\rm d}$ as

$$\Delta m_{\rm d} = 0.444 \pm 0.029\ ^{+0.020}_{-0.017}\ \text{ps}^{-1}\ ,$$

where the first error is essentially statistical and the second is systematic. Note that all constrained parameters were consistent with the constraints to within one standard deviation, except $f_{\rm b\to c\to \ell}$, $f_{\rm uds}$ and $\delta Q_{\rm udsc}$ where the fitted values were larger than the constraint values, but were consistent at the level of two standard deviations.

Origin	Systematic error on Δm_{d} in ps^{-1}
f_{s}	$^{-0.011}_{+0.010}$
f_{baryon}	$^{+0.005}_{-0.004}$
$f_{\mathrm{b}\to\mathrm{c}\to\ell}$	∓ 0.002
f_{c}	± 0.000
f_{uds}	± 0.000
$\langle\tau_{\mathrm{b}}\rangle$	± 0.000
$\tau^{+}/\tau_{\mathrm{d}}$	± 0.004
$\tau_{\mathrm{s}}/\tau_{\mathrm{d}}$	∓ 0.002
$\tau_{\Lambda_{\mathrm{b}}}/\tau_{\mathrm{d}}$	$^{+0.007}_{-0.006}$
δQ_{b}	∓ 0.001
δQ_{mix}	∓ 0.007
$\delta Q_{\mathrm{B}^{+}}$	± 0.006
δQ_{udsc}	∓ 0.003
$f_{\mathrm{D}^{**}}$	± 0.000
Tracking resolution	± 0.004
b fragmentation	± 0.003
Resolution effect of D^{**}	∓ 0.001
Δm_{s} variation	$^{+0.009}_{-0.000}$
Total	$^{+0.020}_{-0.017}$

Table 6: Summary of systematic errors on Δm_{d}

6.2 Study of Δm_s

In order to constrain Δm_s, we consider two different techniques. For the first technique, we plot in Figure 8 the value of $-\Delta \log \mathcal{L}$ as a function of Δm_s, where $\Delta \log \mathcal{L}$ indicates the difference in $\log \mathcal{L}$ relative to the maximum value of $\log \mathcal{L}$. The solid points include the effects of the systematic uncertainties. They were obtained by allowing all parameters, including Δm_d, to vary at each value of Δm_s. To account for systematic errors due to the description of the resolution, four different sets of resolution functions were used. In addition to the default functions, we used the resolution functions obtained without the impact parameter smearing in the Monte Carlo, and those obtained using the Monte Carlo with different fragmentation parameters. A fourth choice of resolution function was obtained by using only semileptonic B_s^0 decays to parametrise sources 5,9,10 and 11 (using the nominal tracking resolution). For each of the four sets of resolution functions the full minimisation of the other parameters was performed at each Δm_s point, giving four distributions of $\Delta \log \mathcal{L}$, with respect to the point of maximum $\mathcal{L}$ relevant to each set, versus Δm_s. The solid points were obtained simply by taking the minimum value of $\Delta \log \mathcal{L}$ from the four choices at each Δm_s point. As a result of this procedure, the points for $\Delta m_s < 1$ ps^{-1} and for $\Delta m_s \geq 3.6$ ps^{-1} are taken from the resolution functions without the impact parameter smearing, while those for 1 ps$^{-1} \leq \Delta m_s < 3.6$ ps^{-1} come from the resolution functions obtained with the modified fragmentation parameters. The value of $\Delta \log \mathcal{L}$ at $\Delta m_s = \infty$ was found to be 2.6 (including systematic errors). A limit on Δm_s is extracted by finding the intersection of these points with a limit curve calculated using a Monte Carlo technique. This technique consisted of performing fast simulations of the data sample, assuming various values of Δm_s. The simulated samples were then analysed in the same way as the data (including the multiparameter fit), and a distribution of $\Delta \log \mathcal{L}$ obtained at each Δm_s point. The limit curve is defined by the value of $\Delta \log \mathcal{L}$ above which lie only 5% of the simulated samples. A total of 6000 samples were simulated, distributed over four values of Δm_s. Three of the limit points and the limit curve, obtained by linear interpolation, are indicated in Figure 8. The fourth limit point is at $\Delta m_s = 50$ ps^{-1}.

We extract a limit $\Delta m_s > 3.1$ ps^{-1} at 95% confidence level. The region 5.0 ps$^{-1} < \Delta m_s <$ 7.6 ps^{-1} is also excluded. The dotted curve shows the result of performing the full minimisation at the global minimum, $\Delta m_s = 3.6$ ps^{-1}, using the default resolution functions, and then scanning through Δm_s while keeping all other parameters fixed. The fitted value of f_s, of particular relevance for Δm_s measurements, was $(11.5 \pm 1.9)\%$.

A second technique for studying Δm_s, known as the amplitude method [28], was also used. The method consists of replacing the $\cos \Delta m_s t'$ term in the physics function with $A \cos \Delta m_s t'$, where A is known as the amplitude. The parameter A may be fitted at each value of Δm_s, and if the value is smaller than unity then the value of Δm_s may be excluded with a confidence that depends only on the value and uncertainty of A. The advantage of such a technique over an exclusion based on $\Delta \log \mathcal{L}$ is that A is measured with errors that are approximately Gaussian. This makes it easy to combine results and compare sensitivities from different analyses or experiments. The calculation of a limit is also relatively straightforward.

For this analysis, A was simply added as an extra parameter to the fit. All systematic uncertainties were handled in the same way as for the Δm_d result. The fitted value of A as a function of Δm_s is shown in Figure 9. To facilitate combination with other results, the central values and a breakdown of the error contributions in steps of 1 ps^{-1} are documented in the

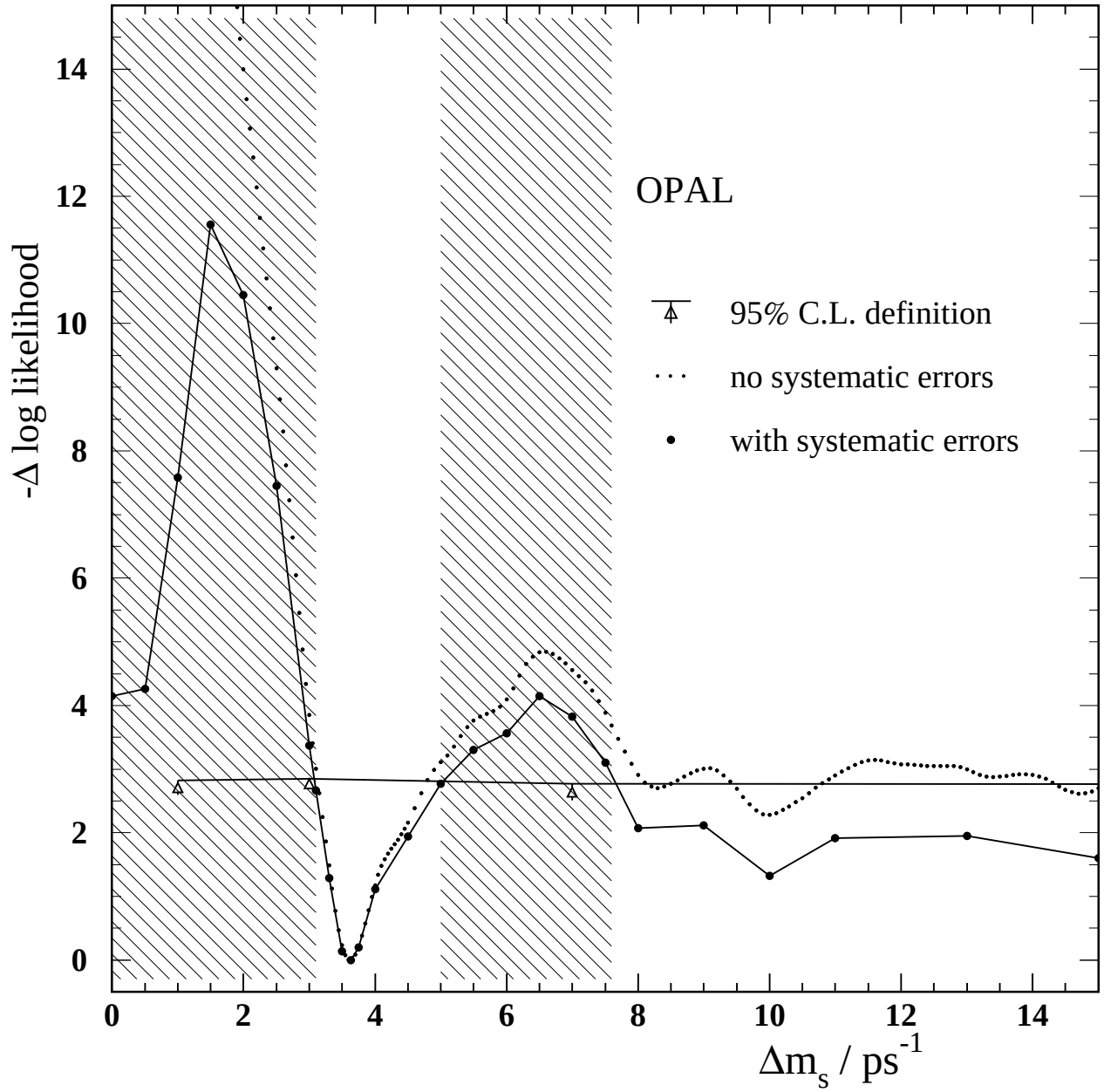

Figure 8: The dotted line shows the distribution of $-\Delta \log \mathcal{L}$ with respect to the maximum value of $\log \mathcal{L}$ as a function of $\Delta m_{\rm s}$, while keeping all other parameters fixed to values optimised at $\Delta m_{\rm s} = 3.63$ ps^{-1}. The solid points include the effects of systematic uncertainties. The open triangles represent the position of the 95% confidence level, and the horizontal line joins together these points, increased by one standard deviation. The hatched region indicates values of $\Delta m_{\rm s}$ excluded at 95% confidence level by this analysis.

Appendix. The results are qualitatively in agreement with the $\Delta \log \mathcal{L}$ method. There is a possible signal near $\Delta m_s = 4$ ps^{-1}, as seen also in the $\Delta \log \mathcal{L}$ plot, where A is close to 1 and significantly separated from 0. Previous measurements [29, 27] exclude this region with a high confidence, so that this excursion is more likely to be a statistical fluctuation. To determine exclusion regions at 95% confidence level, at a given value of Δm_s we represent the measured value of A as a Gaussian distribution function $G(A-\mu, \sigma_A)$, where μ is the central value and σ_A is the measurement error. Two alternative methods are then considered to determine whether the value of Δm_s is excluded:

a) values are excluded where the probability of measuring an amplitude lower than that observed is less than 5%, if that value of Δm_s was the correct one, i.e.

$$\int_1^\infty G(A-\mu, \sigma_A) \mathrm{d}A < 0.05 \, , \tag{19}$$

or

b) the same definition, but limited to the positive region, i.e.

$$\frac{\int_1^\infty G(A-\mu, \sigma_A) \mathrm{d}A}{\int_0^\infty G(A-\mu, \sigma_A) \mathrm{d}A} < 0.05 \, . \tag{20}$$

The first definition gives a true 95% confidence level, in the sense that there is a 5% probability to exclude the true value. However, it is not protected against setting limits well beyond the experimental sensitivity. The second definition makes use of the fact that the predicted value of A lies between 0 and 1, regardless of the value of Δm_s. It is automatically protected against setting limits beyond the sensitivity. For a true value of Δm_s well beyond the sensitivity, method a) would exclude the true value in 5% of the experiments, while for method b) this percentage would tend towards zero.

For method a), excluded regions are defined by $A + 1.645\sigma_A < 1$, where σ_A represents the total error on A. This gives the result $\Delta m_s > 2.9$ ps^{-1} at 95% confidence level. The small region 6.4 ps^{-1} $< \Delta m_s <$ 6.7 ps^{-1} is also excluded. For method b), we find a limit $\Delta m_s > 2.9$ ps^{-1}, and higher Δm_s regions are not excluded. The difference between the two lower limits is 0.03 ps^{-1}. Both results are similar to those obtained from the $\Delta \log \mathcal{L}$ technique.

We define a measure of the sensitivity of this experiment as the value of Δm_s that would be excluded by method a) if A were measured to be 0, i.e. where $1.645\sigma_A = 1$. The sensitivity is 4.8 ps^{-1}.

6.3 Data tests

The plots of R (the fraction of events with $Q_\ell Q_{2jet} < 0$) versus t and $\langle Q_\ell Q_{2jet} \rangle$ versus t shown in Figure 6 are repeated in Figure 10, but restricted to the time windows -0.25 ps $< t <$ 3 ps and -0.5 ps $< t <$ 3 ps respectively. Also shown in these plots are the fitted curves assuming $\Delta m_s = 3.6$ ps^{-1} and $\Delta m_s = 15$ ps^{-1} using the nominal tracking resolution. Calculating the χ^2 summed over both plots (over the full time range) yields values of 44.8 for $\Delta m_s = 3.6$ ps^{-1} and 48.0 for $\Delta m_s = 15$ ps^{-1} for 39 bins in each case. The difference in $\log \mathcal{L}$ between these

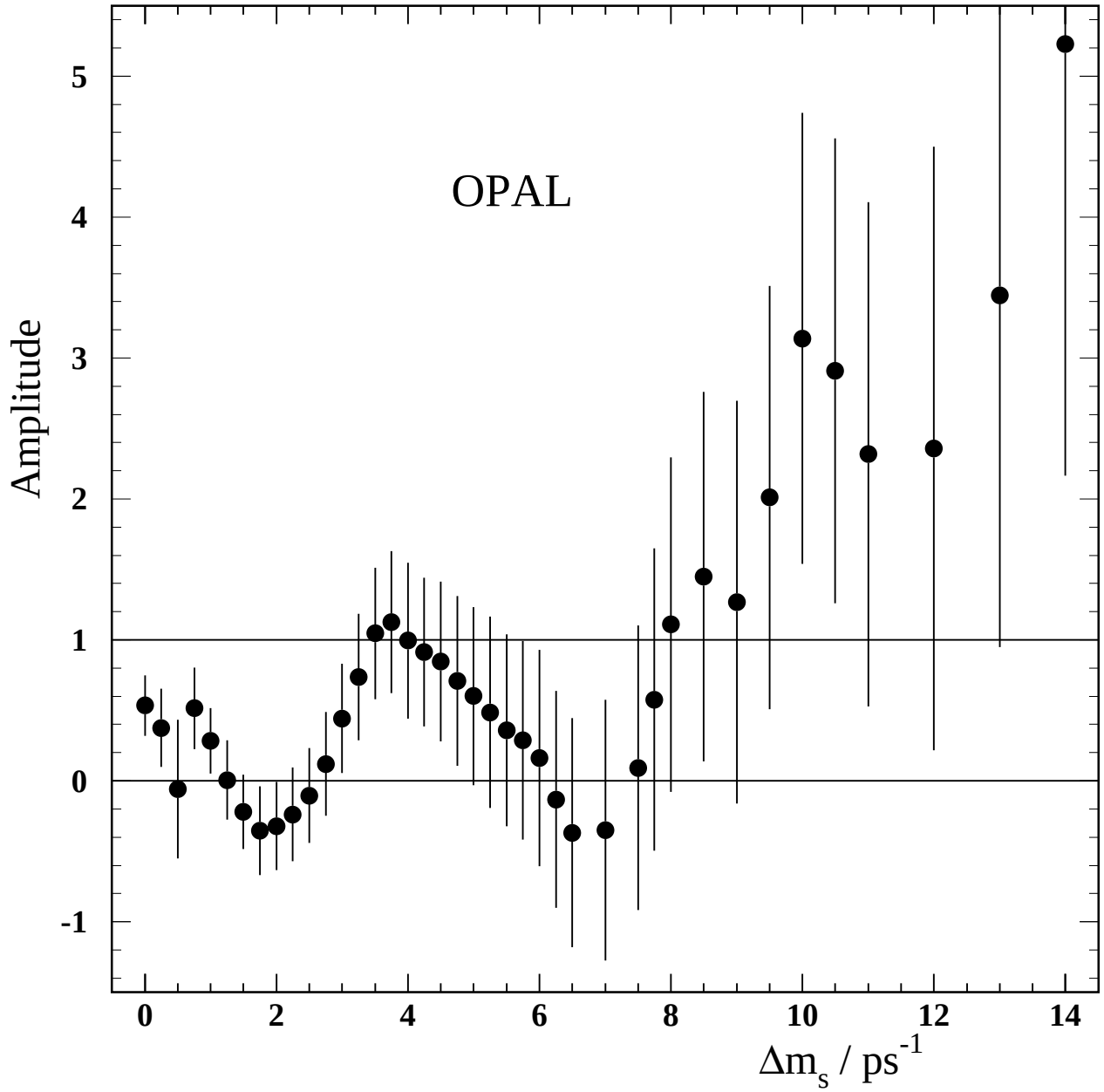

Figure 9: The result of the amplitude fit. The points show the fitted value of the amplitude, A, as a function of $\Delta m_{\rm s}$, and the error bars include all systematic errors.

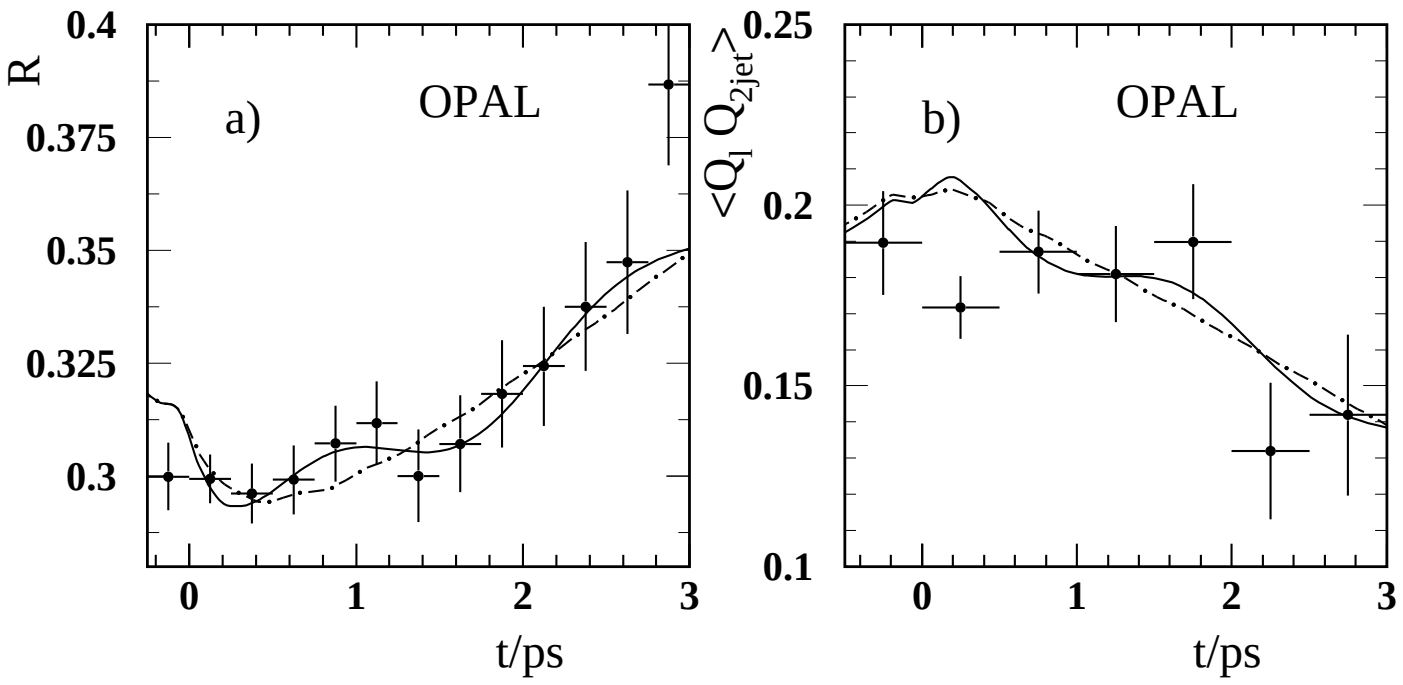

Figure 10: a) The ratio R versus t for data with $|Q_{2jet}| > 2$, restricted to the time window -0.25 ps $< t < 3$ ps. b) The value of $\langle Q_\ell Q_{2jet} \rangle$ versus t for data with $|Q_{2jet}| < 2$, for the time window -0.5 ps $< t < 3$ ps. The solid line shows the result of the fit when $\Delta m_s = 3.6$ ps^{-1}, and the dashed-dotted line corresponds to $\Delta m_s = 15$ ps^{-1}.

two values of Δm_s is 2.5 (again using the nominal tracking resolution), showing a behaviour similar to that of the calculated χ^2 values. This test suggests that the global minimum at $\Delta m_s = 3.6$ ps^{-1} is not an artefact of the fitting procedure, but is rather a property of the data.

To test the stability of the results, the Δm_d fit was repeated using a tighter selection: the α_{kin} cut was changed from 0.7 to 0.85. The fit result was 0.438 ± 0.039 ps^{-1}, consistent with the previous result of 0.444 ± 0.034 ps^{-1}.

6.4 Monte Carlo tests

The multiparameter constrained fit described above was performed on a Monte Carlo sample based on four million hadronic events generated with $\Delta m_d = 0.438$ ps^{-1} and an infinite value of Δm_s, with Δm_s fixed to a large value in the fit. The fitted value for Δm_d was 0.430 ± 0.030 ps^{-1}. The fitted values for three of the parameters, $\langle \tau_b \rangle$, f_{uds} and $f_{b \to c \to \ell}$, were more than 2σ from their true values. If the uncertainty due to the resolution functions and their parametrisation is taken into account, then all values of all parameters are consistent with their true values. A possible bias associated with these parameters was investigated in the data by repeating the fit with all three of these parameters fixed to their nominal values. The result for Δm_d was shifted by $+0.003$ ps^{-1}. The effect on the fitted amplitude for B_s^0 oscillations at $\Delta m_s = 3.75$ ps^{-1} was a shift of 0.18, which is easily covered by the total error of 0.50. The possible bias does not cause a significant problem for the results, and is addressed by resolution function uncertainties.

To test the sensitivity to $\Delta m_{\rm s}$, the single sample of four million simulated events was used to simulate event samples with $\Delta m_{\rm d} = 0.45$ ps^{-1} and a range of values for $\Delta m_{\rm s}$: 1 ps^{-1}, 2 ps^{-1}, 3 ps^{-1}, 4 ps^{-1}, 5 ps^{-1}, 6 ps^{-1}, 8 ps^{-1}, 10 ps^{-1} and 15 ps^{-1}. The values of the fit parameters other than $\Delta m_{\rm s}$ were fixed at their known values in the simulation, and $\log \mathcal{L}$ calculated as a function of $\Delta m_{\rm s}$ for each simulated event sample. The resulting plots of $-\Delta \log \mathcal{L}$ versus $\Delta m_{\rm s}$ (relative to the point of maximum likelihood) for simulated data are shown in Figure 11. It can be seen that $\Delta \log \mathcal{L}$, calculated at the generated value, is in most cases smaller than 2.8, which corresponds roughly to a 95% confidence level. The exceptions are the samples generated with $\Delta m_{\rm s} = 8$ ps^{-1}, where the generated value is just excluded, and $\Delta m_{\rm s} = 15$ ps^{-1}, but note that the samples are statistically correlated with each other. It is interesting to note that in the case of the sample generated with $\Delta m_{\rm s} = 15$ ps^{-1}, an apparent signal would have been seen at a low value of $\Delta m_{\rm s}$. Such cases are properly included in the fast Monte Carlo simulations.

Using the same simulated samples, the equivalent test was performed for the amplitude method. All fit parameters were fixed with the exception of A, which was fitted as a function of $\Delta m_{\rm s}$, for each sample. The results are shown in Figure 12. For the sample generated with $\Delta m_{\rm s} = 8$ ps^{-1}, the generated value of $\Delta m_{\rm s}$ would be excluded by method a), but not by method b). In none of the other samples would the generated $\Delta m_{\rm s}$ value be excluded by either method.

7 Test of CP(T) conservation

The multiparameter fit was repeated with two extra free parameters, $\mathrm{Re}\,\epsilon_{\rm B}$ and $\mathrm{Im}\,\delta_{\rm B}$, with the physics function modified as described in section 5. The results were first tested on four Monte Carlo samples simulated with and without CP and CPT violation. The four Monte Carlo samples are statistically correlated and are each equivalent to four million hadronic events. The results of this test, in which $\Delta m_{\rm s}$ was fixed to a large value (and A fixed to 1), but all other parameters were free to vary, are given in Table 7.

Generated $\mathrm{Re}\,\epsilon_{\rm B}$	Generated $\mathrm{Im}\,\delta_{\rm B}$	Fitted $\mathrm{Re}\,\epsilon_{\rm B}$	Fitted $\mathrm{Im}\,\delta_{\rm B}$
0	0	-0.014 ± 0.009	0.005 ± 0.014
0	0.1	-0.015 ± 0.010	0.096 ± 0.015
0.1	0	$0.077\ ^{+0.012}_{-0.011}$	$-0.002\ ^{+0.015}_{-0.014}$
0.2	0	$0.177\ ^{+0.018}_{-0.016}$	-0.013 ± 0.016

Table 7: Results of fits for $\mathrm{Re}\,\epsilon_{\rm B}$ and $\mathrm{Im}\,\delta_{\rm B}$ using simulated data. There is a strong statistical correlation between the different samples.

The result of the fit to the data, with $\Delta m_{\rm s}$ fixed to 15 ps^{-1}, was

$$\begin{aligned} \mathrm{Re}\,\epsilon_{\rm B} &= -0.006 \pm 0.010 \\ \mathrm{Im}\,\delta_{\rm B} &= -0.020 \pm 0.017\ . \end{aligned}$$

The distribution of $R_{\rm lept}$, the fraction of leptons that are negatively charged, versus reconstructed time is shown in Figure 13 for the data, with the fit result superimposed. In this figure, the data is divided into four categories according to the sign of $Q_\ell Q_{2jet}$ and whether

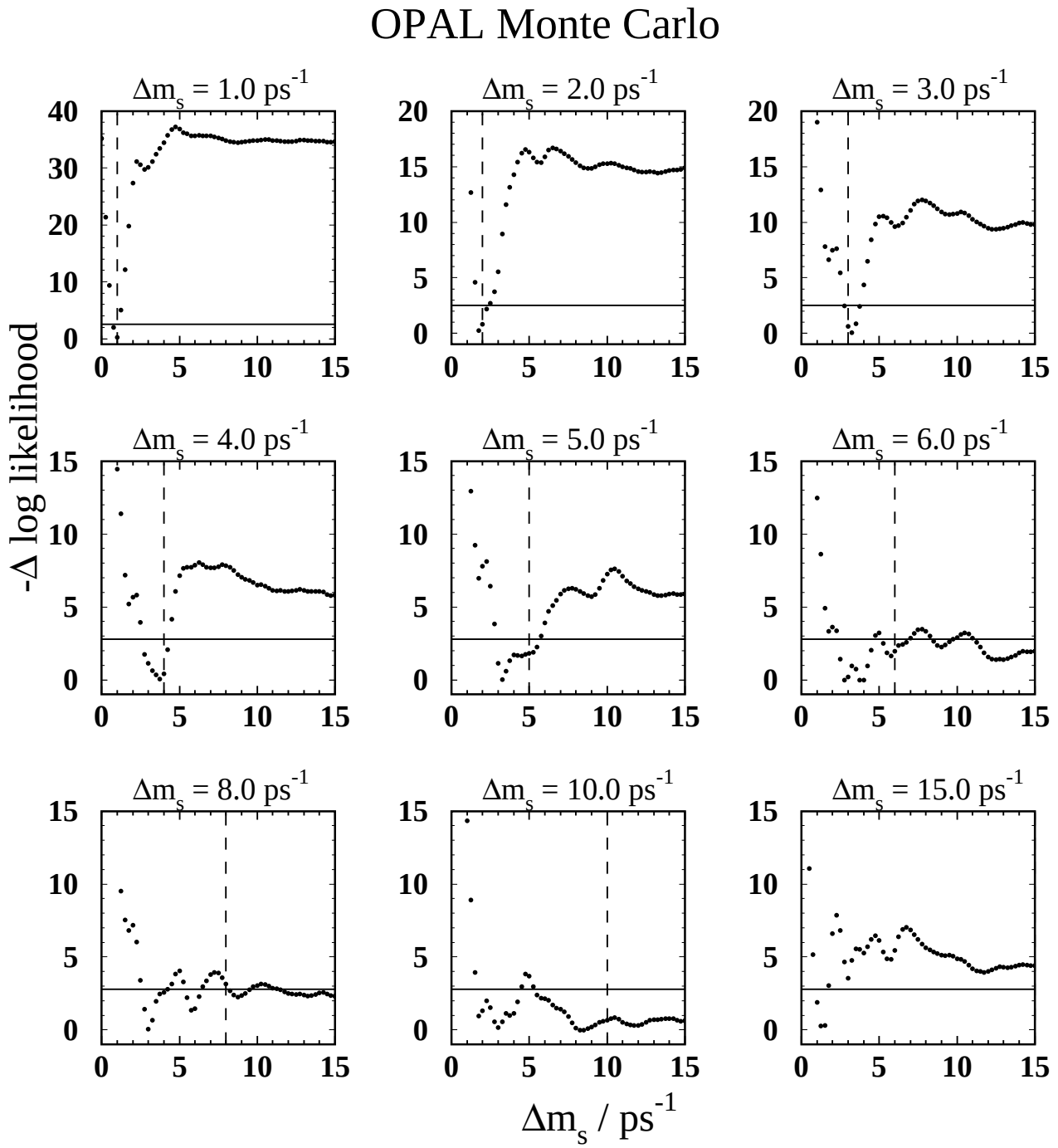

Figure 11: The value of $-\Delta \log \mathcal{L}$, relative to the maximum value of $\log \mathcal{L}$, as a function of $\Delta m_{\rm s}$ for data simulated using nine different $\Delta m_{\rm s}$ values, indicated by the dashed line in each case. All other parameters in the likelihood calculation were fixed. The Monte Carlo event statistics are equivalent to 4 million hadronic Z^0 decays. Note that the different values of $\Delta m_{\rm s}$ are not statistically independent. Horizontal lines are drawn on each plot at $-\Delta \log \mathcal{L} = 2.8$, corresponding roughly to a 95% confidence level.

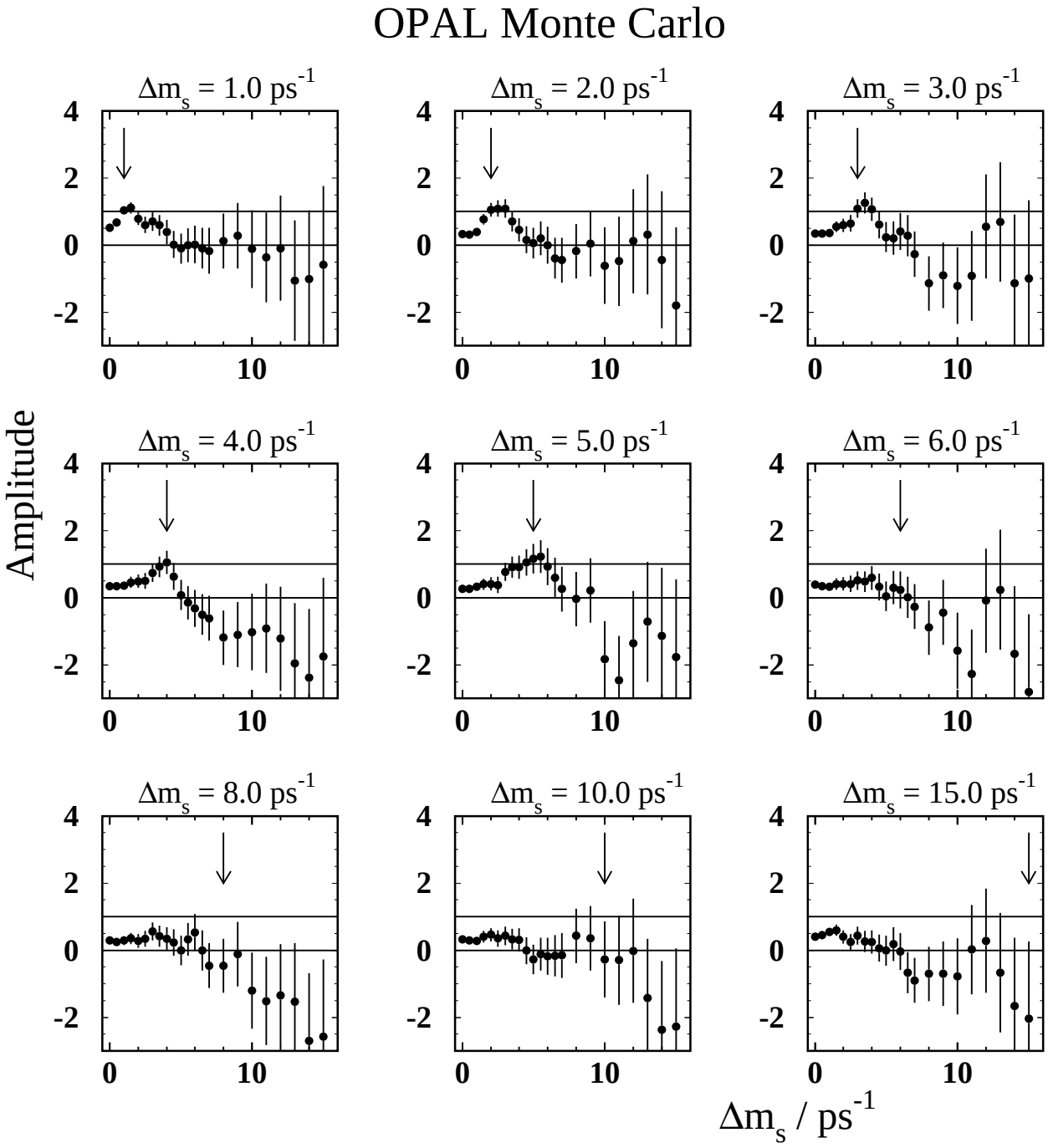

Figure 12: The fitted value of A as a function of $\Delta m_{\rm s}$ for data simulated using nine different $\Delta m_{\rm s}$ values, indicated by the arrow in each case. All parameters other than A were fixed in the fit. The Monte Carlo event statistics are equivalent to 4 million hadronic Z^0 decays, but the nine samples are statistically correlated.

$|Q_{2jet}|$ is smaller or larger than 2. Note that, following equation 10, the data with $Q_\ell Q_{2jet} < 0$ (enhanced in mixed events) are more sensitive to $\mathrm{Re}\,\epsilon_\mathrm{B}$, while the data with $Q_\ell Q_{2jet} > 0$ are more sensitive to $\mathrm{Im}\,\delta_\mathrm{B}$. For comparison, the predicted curves assuming $\mathrm{Re}\,\epsilon_\mathrm{B} = 0.1$, $\mathrm{Im}\,\delta_\mathrm{B} = 0$ and also $\mathrm{Re}\,\epsilon_\mathrm{B} = 0$, $\mathrm{Im}\,\delta_\mathrm{B} = 0.1$ are included in the figure. These curves were obtained keeping all other parameters fixed at their fitted values.

As in the case of the Δm_d analysis, the errors quoted contain both statistical and systematic components. The systematic errors are shown in Table 8, including the errors from the resolution function, calculated as in the Δm_d analysis. The uncertainty due to the weighting function $w(|Q_{2jet}|)$ is also indicated, estimated by shifting the jet charge by 0.06 for Monte Carlo simulated with $\chi = 0.5$ in the opposite jet. Such a shift causes a 10% change in $w(|Q_{2jet}|)$.

Origin	Error on $\mathrm{Re}\,\epsilon_\mathrm{B}$	Error on $\mathrm{Im}\,\delta_\mathrm{B}$	Error on $\mathrm{Re}\,\epsilon_\mathrm{B}$, $\mathrm{Im}\,\delta_\mathrm{B} = 0$
f_s	± 0.000	± 0.000	± 0.000
f_baryon	± 0.002	± 0.002	± 0.000
$f_{\mathrm{b}\to\mathrm{c}\to\ell}$	± 0.000	± 0.000	± 0.000
f_c	± 0.000	± 0.000	± 0.000
f_uds	± 0.000	∓ 0.001	± 0.000
$\langle\tau_\mathrm{b}\rangle$	∓ 0.001	∓ 0.001	± 0.000
τ^+/τ_d	± 0.000	± 0.001	± 0.000
$\tau_\mathrm{s}/\tau_\mathrm{d}$	∓ 0.001	± 0.000	± 0.000
$\tau_{\Lambda_\mathrm{b}}/\tau_\mathrm{d}$	∓ 0.001	∓ 0.001	± 0.000
δQ_b	± 0.000	± 0.000	± 0.000
δQ_mix	± 0.001	± 0.001	± 0.000
δQ_{B^+}	± 0.001	± 0.002	± 0.000
δQ_udsc	± 0.001	± 0.001	± 0.000
$f_{\mathrm{D}^{**}}$	± 0.000	± 0.000	± 0.000
Tracking resolution	± 0.001	± 0.001	± 0.000
b fragmentation	± 0.001	± 0.002	± 0.000
Resolution effect of D^{**}	± 0.000	± 0.000	± 0.000
Δm_s variation	± 0.000	± 0.000	± 0.000
$w(\|Q_{2jet}\|)$	± 0.001	± 0.000	± 0.000
Jet charge asymmetry	± 0.004	± 0.003	± 0.003
Lepton charge asymmetry	± 0.001	± 0.001	± 0.001
Momentum asymmetry	± 0.001	± 0.001	± 0.001
Lepton background	± 0.002	± 0.003	± 0.001
$\cos\theta$ asymmetry	± 0.000	± 0.000	± 0.000
Total	± 0.006	± 0.006	± 0.003

Table 8: Summary of systematic errors on $\mathrm{Re}\,\epsilon_\mathrm{B}$ and $\mathrm{Im}\,\delta_\mathrm{B}$. The fourth column gives the systematic errors on $\mathrm{Re}\,\epsilon_\mathrm{B}$ when $\mathrm{Im}\,\delta_\mathrm{B}$ is fixed to 0.

In addition to these uncertainties, extra sources of error that affect only the CP(T) param-

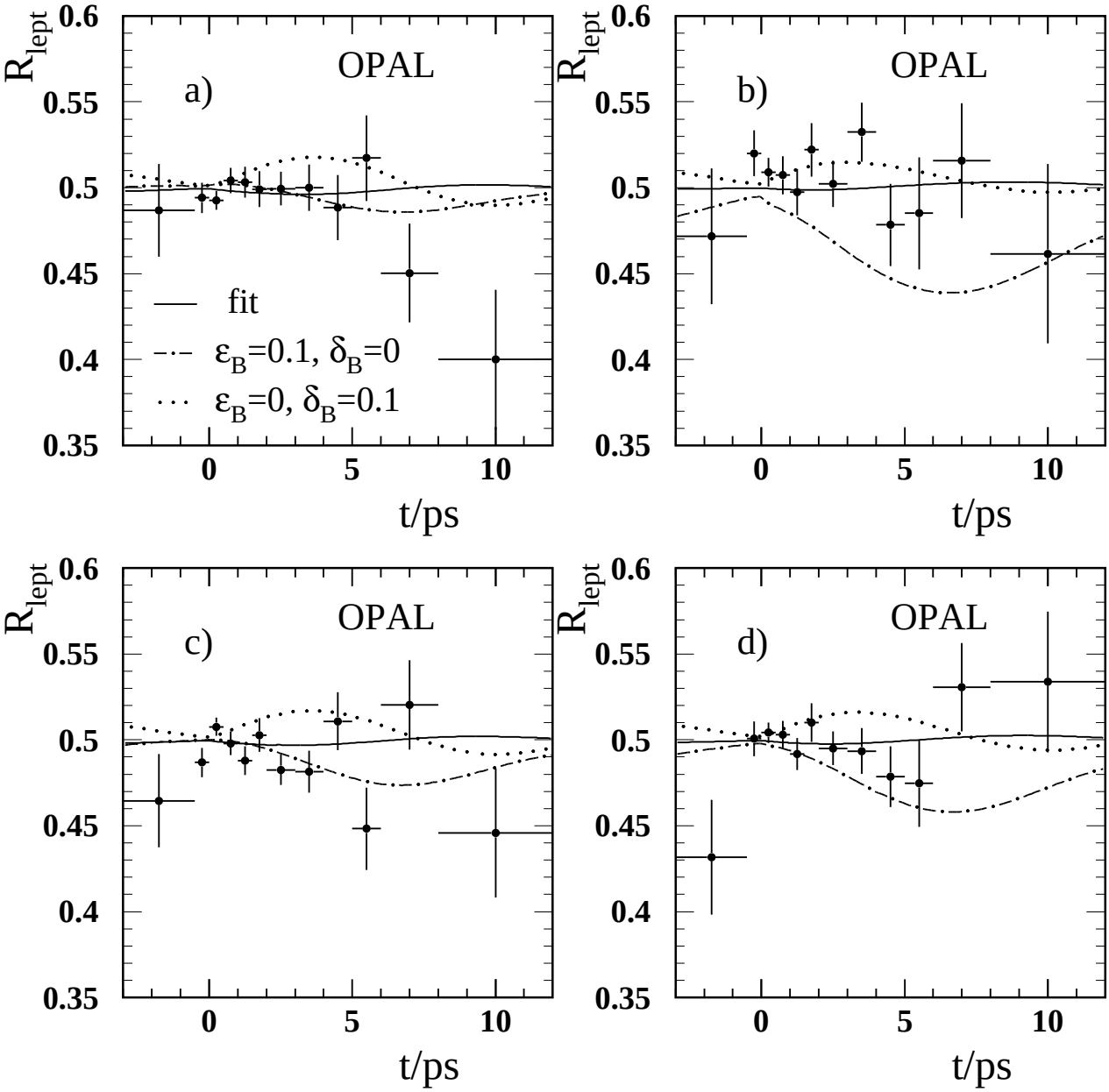

Figure 13: The distribution of $R_{\rm lept}$ versus reconstructed time for the data, with the result of the CPT fit superimposed. The data is divided into four categories : a) $Q_\ell Q_{2jet} > 0$ and $|Q_{2jet}| > 2$, b) $Q_\ell Q_{2jet} < 0$ and $|Q_{2jet}| > 2$, c) $Q_\ell Q_{2jet} > 0$ and $|Q_{2jet}| < 2$, d) $Q_\ell Q_{2jet} < 0$ and $|Q_{2jet}| < 2$. Also shown are the predicted curves for $\mathrm{Re}\,\epsilon_{\rm B} = 0.1$, $\mathrm{Im}\,\delta_{\rm B} = 0$ and for $\mathrm{Re}\,\epsilon_{\rm B} = 0$, $\mathrm{Im}\,\delta_{\rm B} = 0.1$.

eters had to be considered. Firstly, the mean jet charge for produced b quarks is not exactly opposite that for produced $\bar{\mathrm{b}}$ quarks. This is caused by a slight asymmetry in the jet chamber in the efficiency to detect low momentum positively and negatively charged tracks. The asymmetry arises from the geometry of the detector and is therefore simulated in the Monte Carlo. The mean jet charge, averaged over b and $\bar{\mathrm{b}}$ quarks, is found to be $+0.020 \pm 0.006$, where the error is statistical only. This result was checked by studying the charge asymmetry for tracks in hadronic events for both the data and the Monte Carlo. The mean jet charge could then be calculated by weighting the charge asymmetry appropriately as a function of momentum, according to the contribution to the jet charge. Consistent results were obtained whether the weighting was determined from data or Monte Carlo. The resulting mean jet charge values were 0.008 for data and 0.013 for Monte Carlo. This calculated Monte Carlo result is consistent with the value directly observed in the Monte Carlo. The final value for the data is determined by scaling 0.008 by 0.020/0.013, assigning an error of 0.006 due to Monte Carlo statistics, and 0.008 due to the discrepancy seen between Monte Carlo and data, to give 0.012 ± 0.010. This tracking asymmetry could also have a minor effect on the efficiency for selecting leptons (required to have $p > 2$ GeV/c). In this case, the statistics of the Monte Carlo are insufficient to investigate the effect directly. The effect was checked by studying inclusive tracks, passing the same track quality cuts as the leptons, as a function of p. A possible asymmetry of 6×10^{-4} was deduced for a value of $\langle 1/p \rangle = 0.14$ GeV^{-1}, corresponding to the lepton sample. This was assigned as a systematic uncertainty. Another cause of uncertainty would be an asymmetry in the momentum measurements for positive and negative tracks, which could be caused by a slight rotation of the outside of jet chamber relative to the inside. This effect was investigated by studying $\mathrm{Z}^0 \to \mu^+\mu^-$ events in the data. A difference in $\langle 1/p \rangle$ of $(7 \pm 2) \times 10^{-5}$ GeV^{-1} was observed between μ^- and μ^+ particles. Such a shift could cause a lepton selection asymmetry of 5×10^{-4}, assigned as a systematic error.

The results are also sensitive to a charge asymmetry in the lepton background. This asymmetry was studied in the data using electron and muon candidates that just failed the lepton selection criteria. The charge asymmetry was found to be $(1.9 \pm 0.7)\%$, with the largest component due to muon candidates resulting from non-interacting kaons and kaon punchthrough. The central values quoted above were corrected for this effect.

Finally, a $\cos\theta$ asymmetry for lepton identification in the detector would cause a charge asymmetry through the $\mathrm{Z} \to \mathrm{b\overline{b}}$ forward-backward asymmetry, measured by OPAL to be $(9.06 \pm 0.51 \pm 0.23)\%$ at the Z^0 peak [30]. CP(T) violation would not induce a $\cos\theta$ asymmetry. A lepton $\cos\theta$ asymmetry of $(-1.7 \pm 0.3)\%$ (more leptons at $\cos\theta < 0$) was observed in the data. This can be understood as due to an observed average shift of about +0.5 cm of the beam spot along the z-axis relative to the centre of the detector. The central values of $\mathrm{Re}\,\epsilon_\mathrm{B}$ and $\mathrm{Im}\,\delta_\mathrm{B}$ quoted above were adjusted by -0.002 and -0.001, respectively, for this asymmetry and 20% (representing the relative error on the $\cos\theta$ asymmetry) of the shifts taken as systematic error.

Splitting the fit errors into their statistical and systematic components and including the extra systematic errors described above, the final results are :

$$\begin{aligned} \mathrm{Re}\,\epsilon_\mathrm{B} &= -0.006 \pm 0.010 \pm 0.006 \\ \mathrm{Im}\,\delta_\mathrm{B} &= -0.020 \pm 0.016 \pm 0.006\ . \end{aligned}$$

These results neglect CP violation in the B_s^0 system. The sensitivity of the results to $\mathrm{Re}\,\epsilon_{\mathrm{B}_\mathrm{s}^0}$, where $\epsilon_{\mathrm{B}_\mathrm{s}^0}$ is ϵ for the B_s^0 system, was gauged by repeating the fit assuming a large CP asymmetry,

$\mathrm{Re}\,\epsilon_{\mathrm{B}^0_\mathrm{s}} = -0.05$. The value of $\mathrm{Re}\,\epsilon_\mathrm{B}$ was shifted by $+0.015$, while $\mathrm{Im}\,\delta_\mathrm{B}$ was shifted by $+0.006$. Note that the influence of $\mathrm{Im}\,\delta_{\mathrm{B}^0_\mathrm{s}} \neq 0$ on the results is negligible, because the effect is smeared out by the rapid oscillations (see equation 10).

CPT is usually assumed to be a good symmetry, i.e. $\delta_\mathrm{b} = 0$. In the results presented above, there is a correlation of order $+30\%$ between the $\mathrm{Re}\,\epsilon_\mathrm{B}$ and $\mathrm{Im}\,\delta_\mathrm{B}$ results, so we can obtain more precise $\mathrm{Re}\,\epsilon_\mathrm{B}$ results if $\mathrm{Im}\,\delta_\mathrm{B}$ is set to 0. The fit was repeated with $\mathrm{Im}\,\delta_\mathrm{B} = 0$ to give

$$\mathrm{Re}\,\epsilon_\mathrm{B} = 0.002 \pm 0.007 \ ,$$

where the fit contains both statistical and systematic errors. The systematic error calculation was performed as described above, and the errors are included in Table 8. The final result is

$$\mathrm{Re}\,\epsilon_\mathrm{B} = 0.002 \pm 0.007 \pm 0.003 \ .$$

In this case, the effect of $\mathrm{Re}\,\epsilon_{\mathrm{B}^0_\mathrm{s}} = -0.05$ causes a shift of $+0.013$ in $\mathrm{Re}\,\epsilon_\mathrm{B}$.

8 Conclusions

A sample of inclusive lepton events was used to study B^0_d and B^0_s oscillations. An estimate of the decay proper time of the inferred b hadron was reconstructed for each lepton candidate, and a jet charge technique was used to tag the produced B flavour. We measure

$$\Delta m_\mathrm{d} = 0.444 \pm 0.029 \ ^{+0.020}_{-0.017} \ \mathrm{ps}^{-1} \ .$$

This result is consistent with previous measurements [24, 25, 31], and represents the most precise result for a single technique. Taking account of the common systematic errors, we combine this measurement with previous OPAL results [24, 25] to give

$$\Delta m_\mathrm{d} = 0.475^{+0.022\ +0.018}_{-0.023\ -0.016} \ \mathrm{ps}^{-1}.$$

The small statistical correlations between the results have a negligible effect.

By studying the behaviour of $\log \mathcal{L}$ as a function of Δm_s, we are able to exclude the regions $\Delta m_\mathrm{s} < 3.1$ ps^{-1} and 5.0 ps$^{-1} < \Delta m_\mathrm{s} < 7.6$ ps^{-1} at 95% confidence level. Using an amplitude method instead, the lower limit of 3.1 ps^{-1} is slightly weakened to 2.9 ps^{-1}, and the region 5.0 ps$^{-1} < \Delta m_\mathrm{s} < 7.6$ ps^{-1} is either only partially excluded or not excluded at all, depending on the details of the confidence level calculation. The lower limit that would be obtained using the amplitude method, were the amplitude measured to be zero, is 4.8 ps^{-1}, a measure of the experimental sensitivity. This result is consistent with previous results [24, 26, 27, 29], of which the most constraining [29] quotes a lower limit of 6.6 ps^{-1} at 95% confidence level.

By studying the charge symmetry of the B^0_d mixing structure, we are able to constrain possible CP and CPT violating effects. We measure simultaneously the indirect CP violation parameter

$$\mathrm{Re}\,\epsilon_\mathrm{B} = -0.006 \pm 0.010 \pm 0.006$$

and the indirect CPT violation parameter

$$\mathrm{Im}\,\delta_\mathrm{B} = -0.020 \pm 0.016 \pm 0.006 \ .$$

If alternatively we invoke CPT symmetry, then we obtain

$$\mathrm{Re}\,\epsilon_{\mathrm{B}} = 0.002 \pm 0.007 \pm 0.003\ .$$

The $\mathrm{Re}\,\epsilon_{\mathrm{B}}$ measurement, whether or not CPT symmetry is invoked, is consistent with, but more precise than, previous measurements from CLEO [32] and CDF [33]. The $\mathrm{Im}\,\delta_{\mathrm{B}}$ result represents the first measurement of this quantity in the B system.

Appendix: Amplitude results

Section 6.2 describes the amplitude results for the Δm_{s} study. We detail in Table 9 the central values of the amplitude and the breakdown of the error contributions in steps of 1 ps^{-1}. This information is essential for a correct combination of the results from this paper with other analyses. The systematic uncertainties for intermediate points may be estimated by interpolation.

Acknowledgements

We particularly wish to thank the SL Division for the efficient operation of the LEP accelerator and for their continuing close cooperation with our experimental group. We thank our colleagues from CEA, DAPNIA/SPP, CE-Saclay for their efforts over the years on the time-of-flight and trigger systems which we continue to use. In addition to the support staff at our own institutions we are pleased to acknowledge the
Department of Energy, USA,
National Science Foundation, USA,
Particle Physics and Astronomy Research Council, UK,
Natural Sciences and Engineering Research Council, Canada,
Israel Science Foundation, administered by the Israel Academy of Science and Humanities,
Minerva Gesellschaft,
Benoziyo Center for High Energy Physics,
Japanese Ministry of Education, Science and Culture (the Monbusho) and a grant under the Monbusho International Science Research Program,
German Israeli Bi-national Science Foundation (GIF),
Direction des Sciences de la Matière du Commissariat à l'Energie Atomique, France,
Bundesministerium für Bildung, Wissenschaft, Forschung und Technologie, Germany,
National Research Council of Canada,
Hungarian Foundation for Scientific Research, OTKA T-016660, T023793 and OTKA F-023259.

Δm_s (ps^{-1})	0	1	2	3	4	5	6	7
A	0.53	0.29	-0.32	0.44	0.99	0.60	0.16	-0.35
σ_A^{stat}	±0.18	±0.19	±0.29	±0.35	±0.46	±0.59	±0.75	±0.91
f_s	±0.09	±0.11	±0.01	∓0.08	∓0.23	∓0.10	∓0.08	±0.00
f_{baryon}	±0.01	±0.01	∓0.04	±0.02	∓0.02	±0.00	±0.02	±0.03
$f_{b\to c\to\ell}$	±0.04	±0.00	∓0.02	∓0.02	∓0.01	∓0.02	∓0.01	±0.00
$f_{B_s^0\to c\to\ell}$	±0.01	±0.00	±0.00	±0.01	±0.04	±0.01	±0.02	±0.03
f_c	±0.00	∓0.01	∓0.01	±0.00	∓0.01	∓0.01	∓0.01	±0.00
f_{uds}	±0.00	±0.01	±0.01	±0.00	±0.01	±0.01	±0.01	±0.00
$\langle\tau_b\rangle$	±0.00	±0.01	±0.00	±0.00	∓0.01	±0.00	±0.00	∓0.01
τ^+/τ_d	∓0.03	∓0.03	±0.01	∓0.01	∓0.01	∓0.01	∓0.02	±0.00
τ_s/τ_d	±0.02	±0.02	±0.00	∓0.03	∓0.01	∓0.02	∓0.01	∓0.03
τ_{Λ_b}/τ_d	∓0.01	±0.01	∓0.02	±0.00	∓0.02	±0.00	±0.00	±0.01
δQ_b	∓0.06	∓0.02	±0.02	∓0.02	∓0.06	±0.00	∓0.01	±0.05
δQ_{mix}	∓0.01	∓0.01	±0.00	∓0.02	∓0.08	∓0.03	∓0.02	±0.01
δQ_{B^+}	∓0.03	∓0.02	∓0.02	±0.02	±0.04	±0.01	±0.01	∓0.04
δQ_{udsc}	∓0.01	±0.00	∓0.05	∓0.07	∓0.09	∓0.10	∓0.10	∓0.11
$f_{D^{**}}$	±0.01	±0.01	±0.00	±0.00	±0.04	±0.01	∓0.01	∓0.01
Tracking resolution	±0.01	±0.03	±0.08	±0.11	±0.15	±0.14	±0.12	±0.01
b fragmentation	±0.00	±0.02	±0.02	±0.02	±0.01	±0.00	±0.01	±0.04
B_s^0 resolution function	±0.01	±0.03	±0.03	±0.01	±0.04	±0.09	±0.01	±0.06
σ_A^{syst}	±0.13	±0.14	±0.12	±0.16	±0.31	±0.23	±0.18	±0.16

Δm_s (ps^{-1})	8	9	10	11	12	13	14	15
A	1.11	1.27	3.14	2.32	2.36	3.45	5.23	8.90
σ_A^{stat}	±1.06	±1.25	±1.43	±1.69	±1.97	±2.26	±2.64	±3.01
f_s	∓0.18	∓0.04	∓0.46	∓0.09	∓0.49	±0.00	∓0.71	∓1.26
f_{baryon}	∓0.03	∓0.01	∓0.12	±0.03	∓0.07	±0.00	∓0.09	∓0.41
$f_{b\to c\to\ell}$	±0.00	∓0.03	∓0.04	∓0.01	∓0.01	∓0.04	∓0.12	∓0.14
$f_{B_s^0\to c\to\ell}$	±0.03	±0.02	±0.03	±0.01	±0.01	±0.01	±0.01	±0.05
f_c	∓0.03	∓0.02	∓0.07	∓0.04	∓0.04	∓0.03	∓0.13	∓0.23
f_{uds}	±0.03	±0.01	±0.07	±0.03	±0.04	±0.03	±0.13	±0.22
$\langle\tau_b\rangle$	∓0.01	∓0.01	±0.01	±0.00	±0.02	∓0.01	±0.00	±0.01
τ^+/τ_d	±0.00	∓0.04	±0.00	±0.01	∓0.02	∓0.01	±0.02	±0.02
τ_s/τ_d	±0.00	∓0.09	±0.04	∓0.03	∓0.01	∓0.04	∓0.10	±0.02
τ_{Λ_b}/τ_d	∓0.01	∓0.02	±0.00	±0.02	±0.04	±0.00	±0.04	∓0.07
δQ_b	∓0.01	±0.01	∓0.07	±0.02	∓0.10	±0.02	∓0.11	∓0.33
δQ_{mix}	∓0.06	∓0.03	∓0.12	∓0.03	∓0.13	∓0.03	∓0.18	∓0.38
δQ_{B^+}	±0.01	±0.02	±0.05	±0.04	±0.08	±0.02	±0.03	±0.23
δQ_{udsc}	∓0.12	∓0.14	∓0.14	∓0.17	∓0.20	∓0.19	∓0.21	∓0.23
$f_{D^{**}}$	±0.01	±0.01	±0.00	∓0.03	∓0.02	±0.02	±0.04	±0.04
Tracking resolution	±0.02	±0.01	±0.06	±0.06	±0.18	±0.29	±0.45	±0.61
b fragmentation	±0.38	±0.47	±0.31	±0.10	±0.45	±0.79	±0.61	±0.43
B_s^0 resolution function	±0.31	±0.45	±0.38	±0.52	±0.55	±0.59	±1.07	±1.56
σ_A^{syst}	±0.55	±0.68	±0.72	±0.58	±0.93	±1.05	±1.54	±2.29

Table 9: Amplitude results with the breakdown of systematic errors.

References

[1] V.A. Kostelecky and R. Potting, Phys. Rev. **D 51** (1995) 3923.

[2] A. Ali and D. London, Z. Phys. **C 65** (1995) 431, and references therein.

[3] Y. Nir, Phys. Lett. **B 327** (1994) 85.

[4] A. Acuto and D. Cocolicchio, Phys. Rev. **D 47** (1993) 3945.

[5] D. Cocolicchio and L. Maiani, Phys. Lett. **B 291** (1992) 155.
J. Gerard and T. Nakada, Phys. Lett. **B 261** (1991) 474.
J. Liu and L. Wolfenstein, Phys. Lett. **B 197** (1987) 537.

[6] L. Wolfenstein, Phys. Rev. Lett. **51** (1983) 1945.

[7] CPLEAR Collaboration, R. Adler *et al.* and J. Ellis *et al.*, Phys. Lett. **B 364** (1995) 239.

[8] V.A. Kostelecky and R. Potting, Nucl. Phys. **B 359** (1991) 545.

[9] V.A. Kostelecky and R. Van Kooten, Phys. Rev. **D 54** (1996) 5585.

[10] OPAL Collaboration, K. Ahmet *et al.*, Nucl. Inst. and Meth. **A 305** (1991) 275.

[11] P. Allport *et al.*, Nucl. Inst. and Meth. **A 324** (1993) 34;
P. Allport *et al.*, Nucl. Inst. and Meth. **A 346** (1994) 476.

[12] T. Sjöstrand, Comp. Phys. Comm. **39** (1986) 347;
M. Bengtsson and T. Sjöstrand, Comp. Phys. Comm. **43** (1987) 367;
M. Bengtsson and T. Sjöstrand, Nucl. Phys. **B 289** (1987) 810;
T. Sjöstrand, CERN-TH/6488-92.

[13] OPAL Collaboration, G. Alexander *et al.*, Z. Phys. **C 69** (1996) 543.

[14] J. Allison *et al.*, Nucl. Instrum. Methods **A 317** (1992) 47.

[15] Particle Data Group, 'Review of Particle Physics', Phys. Rev. **D54** (1996) 1.

[16] C. Peterson, D. Schlatter, I. Schmitt and P. Zerwas, Phys. Rev. **D 27** (1983) 105.

[17] OPAL Collaboration, G. Alexander *et al.*, Phys. Lett. **B 364** (1995) 93;
ALEPH Collaboration, D. Buskulic *et al.*, Phys. Lett. **B 357** (1995) 699.

[18] OPAL Collaboration, P. Acton *et al.*, Z. Phys. **C 58** (1993) 523.

[19] OPAL Collaboration, R. Akers *et al.*, Z. Phys. **C 60** (1993) 199.

[20] D. Bardin *et al.*, *ZFITTER, An Analytical Program for Fermion Pair Production in* e^+e^- *Annihilation*, CERN-TH/6443-92.
For this prediction, the Z^0, top quark, and Higgs boson masses are set to $M_{Z^0} = 91.18$ GeV, $M_{\rm top} = 150$ GeV and $M_{\rm Higgs} = 300$ GeV, and $\alpha_s = 0.12$.

[21] OPAL Collaboration, K. Ackerstaff *et al.*, CERN-PPE/96-137, accepted by Z. Phys. C.

[22] OPAL Collaboration, G. Alexander *et al.*, Z. Phys. **C 52** (1991) 175.

[23] OPAL Collaboration, R. Akers *et al.*, Z. Phys. **C 63** (1994) 197.
The jet finding parameters ϵ and R were set to 5.0 GeV and 0.65, respectively.

[24] OPAL Collaboration, R. Akers *et al.*, Z. Phys. **C 66** (1995) 555.

[25] OPAL Collaboration, R. Akers *et al.*, Phys. Lett. **B 327** (1994) 411;
OPAL Collaboration, G. Alexander *et al.*, Z. Phys. **C 72** (1996) 377.

[26] ALEPH Collaboration, D. Buskulic *et al.*, Phys. Lett. **B 322** (1994) 441.

[27] ALEPH Collaboration, D. Buskulic *et al.*, Phys. Lett. **B 356** (1995) 409.

[28] H.G. Moser and A. Roussarie, Nucl. Instr. and Meth. **A 384** (1997) 491.

[29] ALEPH Collaboration, D. Buskulic *et al.*, Phys. Lett. **B 377** (1996) 205.

[30] OPAL Collaboration, G. Alexander *et al.*, Z. Phys, **C 70** (1996) 357.

[31] ALEPH Collaboration, D. Buskulic *et al.*, Phys. Lett. **B 313** (1993) 498;
OPAL Collaboration, R. Akers *et al.*, Phys. Lett. **B 336** (1994) 585;
DELPHI Collaboration, P. Abreu *et al.*, Phys. Lett. **B 338** (1994) 409;
DELPHI Collaboration, P. Abreu *et al.*, Z. Phys. **C 72** (1996) 17;
L3 Collaboration, M. Acciarri *et al.*, Phys. Lett. **B 383** (1996) 487;
ALEPH Collaboration, D. Buskulic *et al.*, CERN-PPE/96-102, submitted to Z. Phys. C.

[32] CLEO Collaboration, J. Bartelt *et al.*, Phys. Rev. Lett. **71** (1993) 1680.

[33] CDF Collaboration, F. Abe *et al.*, Phys. Rev. **D 55** (1997) 2546.